Immune priming in the insect gut: a dynamic response revealed by ultrastructural and transcriptomic changes

Short title: Gut response upon insect immune priming

Moritz Baur[1], Nora K. E. Schulz[1], Lilo Greune[2], Zoe M. Länger[1], Jürgen Eirich[3], Iris Finkemeier[3], Robert Peuß[1], Petra Dersch[2], Joachim Kurtz[1, 4*]

[1] Institute for Evolution and Biodiversity, University of Münster, Hüfferstrasse 1, 48149 Münster, Germany

[2] Center for Molecular Biology of Inflammation, University of Münster, Von-Esmarch-Strasse 56, 48149 Münster, Germany

[3] Institute of Plant Biology and Biotechnology, University of Münster, Schlossplatz 7, 48143 Münster, Germany

[4] Joint Institute for Individualization in a Changing Environment, University of Münster and Bielefeld University

*Corresponding author: Joachim Kurtz; joachim.kurtz@uni-muenster.de

OrcID

Moritz Baur: 0000-0002-0575-3250

Nora Schulz: 0000-0003-3681-720X

Lilo Greune: 0000-0002-6228-4657

Zoe Länger: 0009-0009-4110-6593

Jürgen Eirich: 0000-0003-0963-1872

Iris Finkemeier: 0000-0002-8972-4026

Robert Peuß: 0000-0002-9716-6650

Petra Dersch: 0000-0001-8177-3280

Joachim Kurtz: 0000-0002-7258-459X

Author contributions

JK, MB and NKES conceptualized the experiments. JK obtained the funding and administered the project. MB, LG, ZML and JE were involved in the investigation. MB, NKES, LG and JE curated the data and performed the formal analysis. JK, IF and PD provided necessary resources. MB wrote the original manuscript draft. MB, NKES, LG, ZML, JE, IF, RP, PD and JK wrote and revised the manuscript and approved the final version for publishing.

Abstract

Research on forms of memory in innate immune systems has recently gained momentum with the study of trained immunity in vertebrates and immune priming in invertebrates. Immune priming provides protection against previously encountered pathogens. However, causes and mechanisms of immune priming are still not well understood in most organisms. In this work, we combine RNA sequencing with transmission electron microscopy to investigate the dynamic processes during priming in the gut of a well-established model for oral immune priming, consisting of the host *Tribolium castaneum* and its entomopathogen *Bacillus thuringiensis tenebrionis (Btt)*. We show that priming with specific, pathogen-derived virulence-relevant factors causes damage in the gut of *T. castaneum* larvae, which leads to an early physiological stress response as well as the upregulation of a specific set of immune genes. This response diminishes over time yet enables the gut to upregulate genes known to interfere with *Btt* virulence when *T. castaneum* larvae are later exposed to infectious *Btt* spores. The identification of these processes increases our understanding of immune priming as a dynamic process where cellular responses in concert with specific gene regulation prepare the gut tissue and thereby enable more efficient protection against infection. Such work can further help us understand the origin and mechanism of innate immune memory.

Author summary

Invertebrate animals do not possess a classical adaptive immune system. And yet, many of these animals show forms of immune memory, collectively called immune priming. In this work, we investigate the causes of oral immune priming in the red flour beetle *Tribolium castaneum* in response to its bacterial entomopathogen *Bacillus thuringiensis tenebrionis*. Primary exposure to *Btt* spent culture media supernatants enables the larvae of *T. castaneum* to better withstand a subsequent infection with infectious *Btt* spores. We show that exposing *T. castaneum* larvae to those supernatants leads to damage in the gut resulting in a strong stress and immune response early after priming and a

58 targeted up-regulation of beneficial genes upon the secondary re-encounter with *Btt*. These results
59 suggest fundamental stress responses can be involved in innate immune memory phenomena, which
60 has implications in translational research across species.

61

62 Introduction

63 Immune systems are a universal feature across the tree of life. As checks and balance systems that
64 discriminate between self and non-self, they allow for protection against harmful pathogens and
65 parasites while reducing self-harm. Immune systems of vertebrate animals have classically been
66 divided into the innate and the adaptive arm. Invertebrates lack the specialized cellular machinery that
67 is needed to mount an adaptive immune response in the classical sense [1, 2]. Over the past decades,
68 this clear separation has been challenged by work on both vertebrate and invertebrate immunity. In
69 vertebrates, innate immune memory that has been denoted 'trained immunity' acts through the
70 rewiring of metabolism and epigenetic imprinting of immune and non-immune (e.g., epithelial) cells
71 [3-6].

72 In invertebrates, numerous studies have described enhanced survival upon infection after a previous
73 encounter with pathogens or their cues, despite the absence of the adaptive immune cellular
74 machinery [7-12]. These observations, usually denoted as immune priming, are widespread across
75 invertebrates and entail many distinct phenomena [13]. Systemic or septic immune priming is achieved
76 by pricking or injecting a host with sublethal doses, inactivated microbes, or immunoreactive cues
77 derived from those microbes before infecting it, in the same way, with living microbes. This route of
78 priming can be specific, providing a survival benefit only if the priming agent is the same as the infecting
79 agent [8, 12, 14-16], or unspecific, providing a benefit during a subsequent infection even if the
80 infecting agent is different from the one used for priming [10]. Immune priming is also possible via the
81 oral route. Like septic immune priming, oral immune priming can be specific depending on the host
82 and microorganism involved [7, 17, 18]. The two different routes of immune priming (septic and oral)

83 likely function via different mechanisms [19], although it has also been reported in some organisms
84 that oral immune priming can protect a host against a subsequent septic infection [20, 21]. Immune
85 priming further is transmittable to subsequent generations, a phenomenon termed transgenerational
86 immune priming [22-25]. While mechanisms of septic immune priming have been studied over the past
87 years, similar work on oral immune priming is still scarce.

88 Immune priming via the oral route is likely a complex process. The microbiome seems to play a role in
89 some species [15, 26, 27]. In mosquitoes and bean bugs, members of the microbiome take an active
90 part by breaching the gut epithelium, thereby stimulating immune responses that provide systemic
91 immunization [15, 27]. In an important model for oral immune priming, the red flour beetle *Tribolium*
92 *castaneum*, a shift in the microbiome composition upon priming has been described [28]. Oral immune
93 priming enables insects to better resist a subsequent infection by ingested pathogens in an
94 environment with high pathogen exposure. When the priming agent is taken up via the oral route, the
95 intestine is the first tissue reacting to the presented stimuli.

96 In the present work, we focus on gut-associated processes of oral immune priming in *T. castaneum*
97 when confronted with its natural entomopathogen *Bacillus thuringiensis tenebrionis* (*Btt*). *B.*
98 *thuringiensis* is a spore-forming gram-positive bacterium. During sporulation, it produces crystal toxins
99 (Cry toxins), which become solubilized upon ingestion by the host and form pores in the gut epithelium
100 [29, 30]. Upon germination, *B. thuringiensis* produces a large number of enzymes and toxins to further
101 damage its hosts' gut tissue, ultimately leading to the death of the host [29, 30]. Once *B. thuringiensis*
102 has exhausted the hosts' nutrients, vegetative cells sporulate, ready to infect the next host [29, 30].
103 Greenwood et al. [31] found that oral immune priming of *T. castaneum* larvae with filter sterilized
104 medium derived from sporulating *Btt* cells leads to a shift in whole-body gene expression profiles,
105 which is still detectable four days later. Several immune genes remain up-regulated in primed hosts
106 upon pathogen exposure, and some genes are distinctly induced by challenge in those animals that
107 only received a prior priming [31]. Moreover, recent work comparing proteomes of filtered growth
108 media supernatants derived from closely related *B. thuringiensis* isolates, that either do or do not lead

109 to priming of *T. castaneum* larvae, enabled the identification of candidate virulence factors that might
110 induce oral immune priming, including the plasmid-encoded Cry3Aa toxin [32].

111 We currently lack a comprehensive view of the associated ultrastructural and physiological changes in
112 the gut that lead to the observed enhanced survival upon priming. Here, we studied ultrastructural
113 changes using transmission electron microscopy together with changes in gene expression using RNA-
114 seq of gut tissue of *T. castaneum* larvae at different time points after oral priming and infection to gain
115 information about the mechanisms contributing to oral immune priming in *T. castaneum*. For these
116 experiments, we made use of an improved control *Btt* strain for priming, which was cured of the Cry-
117 toxin-carrying plasmid to identify bacterial candidate proteins leading to priming. As a result, we
118 provide important insights into mechanisms that might constitute innate immune memory in
119 invertebrates, in interplay with their natural pathogens.

120 # Materials and methods

121 ## Model organisms

122 *T. castaneum* larvae used in this study stem from the Croatia 1 (Cro1) strain [28]. Cro1 was collected in
123 2010 in Croatia and maintained in large groups of non-overlapping generations since then. Larvae were
124 reared on heat-sterilized (75°C for 24 h) wheat flour (Bio Weizenmehl Type 550, dm-drogerie markt
125 GmbH + Co. KG) including 5% Brewer's yeast at 30°C, 70% humidity and a 12 h day/night rhythm.

126 *Bacillus thuringiensis* bv *tenebrionis* (*Btt,* BGSCID4AA1) spores were purchased from the Bacillus
127 Genetic Stock Center of the Ohio State University (USA). *Btt ⊿ p188* (previously denoted Btt – [32]),
128 lacking the 188 kb plasmid, was obtained by serial passage of *Btt* at high temperatures [32].

129 ## Study design

130 To understand the immediate responses following an oral priming treatment and which factors are
131 involved in mounting a successful immune priming response, we combined proteomics data from
132 priming media and larval size measurements, with electron microscopy and RNA-seq approaches (Fig
133 1). 14-day old *T. castaneum* larvae were individually exposed to either medium- (*Bt* growth medium),
134 priming (*Btt*)- or control- (*Btt ⊿ p188*) flour mixes (Priming treatment) in a well of a 96-well plate. After
135 24 hours, larvae were transferred onto PBS flour mixes and left for another four days. Finally, larvae
136 were transferred onto PBS- or *Btt* spore-flour mixes (Challenge treatment). For the size measurement
137 (Fig 1), larvae were randomly sampled before exposure to the treatment diets, and the same larvae
138 were re-sampled before exposure to the challenge treatment. For electron microscopy and RNA-
139 sequencing (Fig 1), gut samples were taken from randomly sampled larvae at three hours and 24 hours
140 post-exposure to the priming treatment as well as four hours post-exposure to the challenge treatment
141 five days after the initial priming. In all experiments, the larvae were kept on the challenge treatment,
142 and survival was recorded for three to five days post-exposure. Finally, the proteomes of spent culture

143 media supernatants derived from *Btt* and *Btt Δ p188* cultures were compared to narrow down the

144 agents causing the immune priming response [32].

145

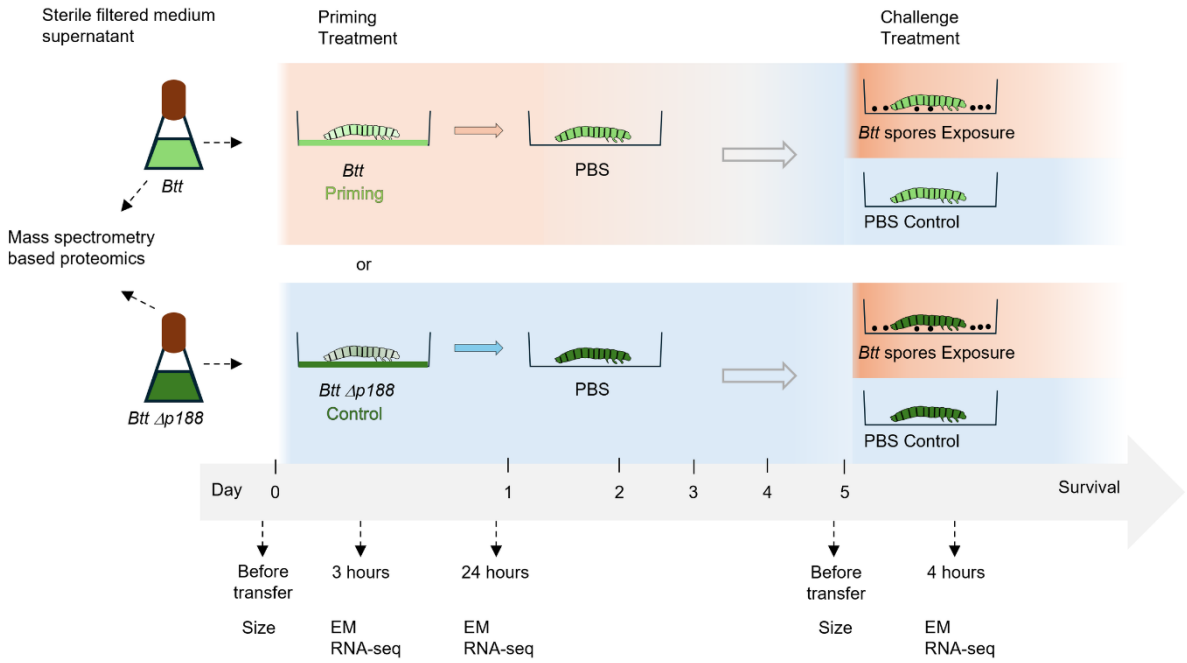

146

147 **Fig 1: Study design.** Before exposure to either priming- (*Btt*) or control (*Btt Δ p188*) supernatant flour mixes
148 (Priming treatment) we measured the size of 14-day-old larvae. Early time-point gut samples were taken at 3
149 hours and 24 hours post-exposure for electron microscopy (EM) and RNA-sequencing (RNA-seq). The remaining
150 larvae were transferred onto PBS flour mixes after 24 hours and left for four more days. Before transferring onto
151 control (PBS)- or exposure (*Btt* spores) flour mixes (Challenge treatment), we measured the size of the same
152 larvae as in the beginning. Four hours after the transfer onto the challenge diets, gut samples were taken for
153 both, EM and RNA-seq again. The sterile-filtered spent culture media supernatants of *Btt* and *Btt Δ p188* that
154 were used for the Priming treatment were also compared regarding their proteome composition with LC MS/MS.

155

156 ## Preparation of diets

157 The spore cultures were prepared as described in Länger and Baur *et al.* (2023) [32] with some
158 modifications. In short, either 50 mL (Priming treatment) or 400 mL (Exposure treatment) *Bt* growth
159 medium was supplemented with 250 µL or 2 mL of a salt solution and 62.5 µL or 250 µL of 1 M $CaCl_2$.
160 Lastly, 1 mL or 5 mL of an overnight *B. thuringiensis* culture (*Btt* or *Btt ∆ p188*) was added.

161 For producing the priming treatments, the sporulated cultures were centrifuged after seven days twice
162 at 2604 rcf for 15 min. The resulting supernatants were filtered through a 0.45 µm filter followed by a
163 0.22 µm filter to remove bacterial spores and vegetative cells. Next, the filtered supernatants were
164 mixed with 0.15 g flour/mL of supernatant, and 10 µL of each mix was pipetted into the wells of a 96-
165 well flat bottom plate (Greiner). Finally, the plates were put to 30°C overnight for drying.

166 To produce the exposure treatment, the sporulated *Btt* cultures were centrifuged as described above.
167 Between the first and second centrifugation the supernatants were discarded, and the spore pellets
168 were washed in 15 mL PBS. The final spore pellets were resuspended in 5 mL PBS, the spores were
169 counted in a Thoma counting chamber (depth 0.02 mm, square area 1/400 mm^2) and the
170 concentrations were adjusted to 1x10^10 spores/mL of PBS. Finally, 0.15 g flour was added to 1 mL of
171 the spore/PBS mix and 10 µL of this final mix was pipetted into the wells of a 96-well flat bottom plate.
172 The plates were put to 30°C overnight for drying.

173 Priming and challenge experiments

174 Priming and challenge of *T. castaneum* larvae was performed as described in [28]. In short, on day 15
175 after oviposition larvae were individualized into the wells of the control or priming diets (*Btt ∆ p188* or
176 *Btt*) or medium control flour diets (0.15 g flour/mL *B. thuringiensis* medium). After 24 hours the larvae
177 were transferred onto PBS diets (0.15 g flour/mL PBS) where they were left for four days at standard
178 conditions (for an overview see Fig 1). Finally, the larvae were transferred onto the exposure (*Btt*
179 spores) or control (PBS) diets, and their survival was recorded daily for five days.

180 # Proteomics

181 To correlate differences in the ability to induce immune priming to differences in the proteomes of the
182 spent growth media supernatants of *Btt* and *Btt Δ p188* cultures, we used four replicate cultures of
183 both bacterial strains (supernatants prepared as in "Preparation of priming and infection diets").
184 Proteins from the supernatant were directly processed for MS analysis following the SP3 protocol, using
185 TCEP (5 mM) and CAA (14 mM) for reduction and alkylation [33]. Proteins were bound to beads by the
186 addition of 100 µL EtOH and washed twice with 80% EtOH. They were digested in 50 mM TEAB, pH 8.5
187 at 37 °C. After the overnight digestion, peptides were dried by vacuum centrifugation and reconstituted
188 in 0.5% TFA and 2% acetonitrile for LC-MS/MS analysis. An EASY-nLC 1200 (Thermo Fisher) coupled to
189 an Exploris 480 mass spectrometer (Thermo Fisher) was used for LC-MS/MS analyses. The peptides
190 were separated on 20 cm frit-less silica emitters (CoAnn Technologies, 0.75 µm inner diameter), packed
191 in-house with reversed-phase ReproSil-Pur C_{18} AQ 1.9 µm resin (Dr. Maisch) and the column was
192 constantly kept at 50 C. Mass spectra were acquired in data-dependent acquisition mode as described
193 in Sindlinger *et al*. [34]. The MaxQuant software version 2.0.3.0 [35] was used to process the raw data
194 and standard settings were used. The LFQ count was 1. The resulting MS/MS spectra were assigned to
195 a custom *Btt* proteome assembly (*Btt* genome kindly provided by Dr. Heiko Liesegang, Institute of
196 Microbiology and Genetics, Georg-August University of Göttingen, unpublished) with default settings
197 and match between runs. Label-free quantification (LFQ) and intensity based absolute quantification
198 (iBAQ) options were enabled.

199 # Larval growth

200 To measure larval growth between priming and challenge time points, larvae were randomly selected
201 before the transfer onto priming or control diets 14 days after oviposition and put onto petri dishes for
202 area measurement. We measured the larval area again in the same way directly before the challenge
203 treatment. The experiment was repeated in 3 blocks, resulting in 132 primed larvae and 135 control
204 larvae being measured. To measure the area of the larvae, pictures were taken with an Olympus SZX12

205 microscope and saved as BigTIFF files. The CellSens Standard software was used to individually measure
206 area in mm^2. A small number of larvae, that had been exposed to priming or control diets, decreased
207 in size, likely due to recent molting.

208 Gut dissection

209 For both, electron microscopy (EM) and mRNA sequencing (RNA-seq), guts of larvae were dissected
210 under sterile conditions after the larvae were immobilized on ice. To obtain guts for EM, larvae were
211 placed into droplets of 15 µL cold PBS and the first and last segments were removed with a scalpel. The
212 guts were then pulled out with forceps and put into 5 mL of fixing solution (see Method section Electron
213 microscopy). Per timepoint and treatment, five guts were dissected for EM. For the guts used for RNA-
214 seq 10 µL RNA-later (Thermo Fisher) was used instead of PBS. For each sample 7 guts were pooled in
215 an 1.5 mL reaction tube containing 100 µL RNA-later on ice. Finally, the access RNA-later was removed
216 , the samples were shock frozen in liquid nitrogen and stored at -80°. Per timepoint and treatment
217 three replicates were used.

218 Transmission electron microscopy

219 Dissected guts were fixed with 4% formaldehyde (Polysciences), 1% glutaraldehyde (Polysciences) in
220 0.1 M cacodylate buffer (Polysciences) pH 7.4 for 30 min and after a change for 3 hours at room
221 temperature. The samples were stored at 4 °C until further processing. After fixation the samples were
222 washed three times with 0.1 M cacodylate buffer (pH 7.4), post-fixed in 1% osmiumtetroxide
223 (Polysciences) in 0.1 M cacodylate buffer at room temperature for one hour and washed with 0.1 M
224 cacodylate buffer. Samples were gradually dehydrated in increasing concentrations (50 %, 70 %, 90 %,
225 96 %, 99.8 %) of ethanol (Roth) for 30 min at each step at 4 °C. After incubation with 100 % propylene
226 oxide (Serva) twice for 10 min, the samples were embedded under vacuum by subsequent incubation.
227 Epoxy resin (Serva) mixed with propylene oxide (1:1, 2:1 each step 4°C overnight), epoxy resin 100 %
228 (2x 2 hours RT) and polymerized in fresh epoxy resin at 60 °C for 72 hours. Ultrathin sections (60-nm)

229 were generated using a Leica EM UC7 ultramicrotome. Sections were poststained with 4 % uranyl
230 acetate (Polysciences) in 25% ethanol and 'Reynold's lead citrate'. Samples were analyzed at 80 kV on
231 a FEI-Tecnai 12 electron microscope (FEI). Images of selected areas were documented with Veleta 4k
232 CCD camera (emsis).

233 RNA-seq

234 To isolate total RNA, dissected gut samples were crushed in 1 mL of TRIzol (Thermo Fisher), sonicated,
235 and centrifuged at 13000 RCF for 5 min. at 4 °C. After a chloroform wash and another round of
236 centrifugation at 10500 RCF for 15 min. at 4 °C, the aqueous phase was collected in EtOH and RNA lysis
237 buffer from the SV Total RNA Isolation kit (Promega), and the manual instruction was followed. The
238 RNA was eluted in 70 µL of RNAse-free water. 15 µL of eluted RNA (~ 80 ng/µL) was sequenced by
239 Novogene (Cambridge, UK) using the Illumina NovaSeq PE150 platform (Paired-end, 150 bp read
240 length). Raw reads were assessed using FastQC software (version 0.11.2) [36]. Adapters were removed
241 and reads were filtered based on criteria such as adapter contamination, nucleotide uncertainty (if >
242 10% of a read), or low-quality nucleotides (if Base Quality < 5 in > 50% of a read). The resulting clean
243 reads were mapped against the *T. castaneum* genome (Tcas5.2.54,
244 http://ftp.ensemblgenomes.org/pub/metazoa/release-54/gtf/tribolium_castaneum/) using hisat2
245 (version 2.0.5) [37], assembled into transcripts or genes with Stringtie (version 1.3.3b) [38] and counted
246 with featureCounts (version 1.5.0-p3) [39].

247 Statistical Analysis

248 All statistical analyses were performed with R (version 4.3.1) [40] implemented in Rstudio (version
249 2023.06.1+524). Visualization of data was carried out using the R package "ggplot2" (version 3.4.4)
250 [41].

251 For the proteome data, $\log_2$ transformation of LFQ intensities was performed. Only protein groups
252 quantified in at least 3 of 4 replicates in at least one treatment supernatant (*Btt* or *Btt* Δ *p188*) were

253 considered for the downstream analysis and missing LFQ values were imputed based on quantile
254 regression using the package “imputeLCMD” (version 2.1). The R package “limma” (version 3.58.1) was
255 used to statistically test for differential expression [42].

256 To statistically assess the influence of priming treatment on the growth of the larvae, measured area
257 was modeled as the response variable explained by time point and treatment (priming or control) as
258 explanatory variables and both, experimental blocks and individuals as random factors using the “lmer”
259 function from the R package “lme4” (version 1.1-35.1) [43]. The model was as follows: Size ~
260 Treatment*Time + (1|Block/Individual). To assess the treatment effect the full model was compared
261 with a reduced model (Size ~ 1 + (1|Block/Individual)) using the “anova” function.

262 For the survival analysis of the larval growth experiment, we applied a Cox proportional hazards model
263 with one random factor using the “coxme” function from the “coxme” package (version 2.2-18.1) [44].
264 The model was as follows: (Surv(Day, Event) ~ Treatment +(1|Replicate)). To assess the treatment
265 effect, the full model was compared to a reduced model: “coxme” (Surv(Day, Event) ~ 1
266 +(1|Experiment), data), using the “ANOVA” function. The medium control was set as the reference. For
267 the survival analysis of the RNA-seq and EM experiments, we applied the “coxph” function from the
268 “survival” package (version 3.5-7) without adding a random factor: (Surv(Day, Event) ~ Treatment). In
269 all cases, treatment (medium, *Btt* or *Btt Δ p188*) was set as the fixed factor, and proportionality of the
270 fixed effect was assessed with the cox.zph() function from the “survival” package. Additionally, the
271 survival curves were plotted using the “survfit” function from the “survival” package [45] and
272 “ggsurvplot” from “ggplot2”.

273 For the RNA-sequencing data, differential gene expression analysis was performed with DESeq2
274 (version 1.20.0) [46], on genes with raw counts greater than 2 in the comparison groups (priming vs.
275 control after 3 hours, 24 hours, 5 days, 5 days + *Btt*). Genes with a log2 fold change > 0.5 or < -0.5 and
276 a False Discovery Rate (FDR, Benjamini-Hochberg) adjusted p-value < 0.05 were considered significantly
277 up-regulated or down-regulated, respectively. GO enrichment analysis was performed using the R

278 package clusterProfiler (version 4.10.0) [47] with a threshold of FDR adjusted $p < 0.05$. Weighted Gene
279 Co-expression Network Analysis was carried out using the R package WGCNA (version 1.72-5) [48].
280 Initially, samples were checked for outliers (hierarchical clustering upon distance matrix computation
281 and PCA), genes with a raw count lower than 10 in 50% of the samples were filtered out, and the
282 remaining reads were variance stabilized using the "vst()" function (DESeq2). A soft thresholding power
283 for gene correlations of 14 was chosen based on high-scale freeness and low mean connectivity. Both
284 network type and TOMtype were set to "signed" to cluster genes that are either co-up- or co-down
285 expressed. To statistically compare the module eigengene values of the different modules between
286 groups, the R package limma (version 3.58.1) was used. Modules with significantly different module
287 eigengene values (FDR adjusted $p < 0.05$) were exported to Cytoscape (version 3.10.1) [49] and
288 visualized with the plug-in ClueGO (version 2.5.10) [50]. Only significantly enriched terms (FDR adjusted
289 $p < 0.05$) were visualized and terms were grouped based on the number of shared genes (Kappa score
290 = 0.4).

291

Results

T. castaneum oral immune priming response in the gut peaks after 24 hours and resembles an infected state

As little is known about the mechanisms of oral immune priming in the insect gut, we here used the *T. castaneum – B. thuringiensis tenebrionis* host-pathogen model to provide insights into this phenomenon. The survival data derived from the present experiments confirm oral immune priming in *T. castaneum:* larvae showed improved survival of *Btt* infection when they were previously exposed to priming diets derived from *Btt* culture supernatants (Estimate = 0.57, $p < 0.001$), but not when exposed to *Btt Δ p188* control diets (Estimate = 1.13, $p = 0.34$) (each compared to *Bt* medium diets, Fig 2A,B, S1 Fig).

The increased survival probability after priming came at the cost of reduced growth in the treated individuals, which can be an indicator of slower development to pupal and adult stages [9]. During the time between priming and challenge exposure, larvae, which were initially of the same size (Fig. 2C, Estimate = 0.02038, $p = 0.6586$) grew significantly less if they received the priming treatment compared to the control (Estimate = -0.13439, $p < 0.001$).

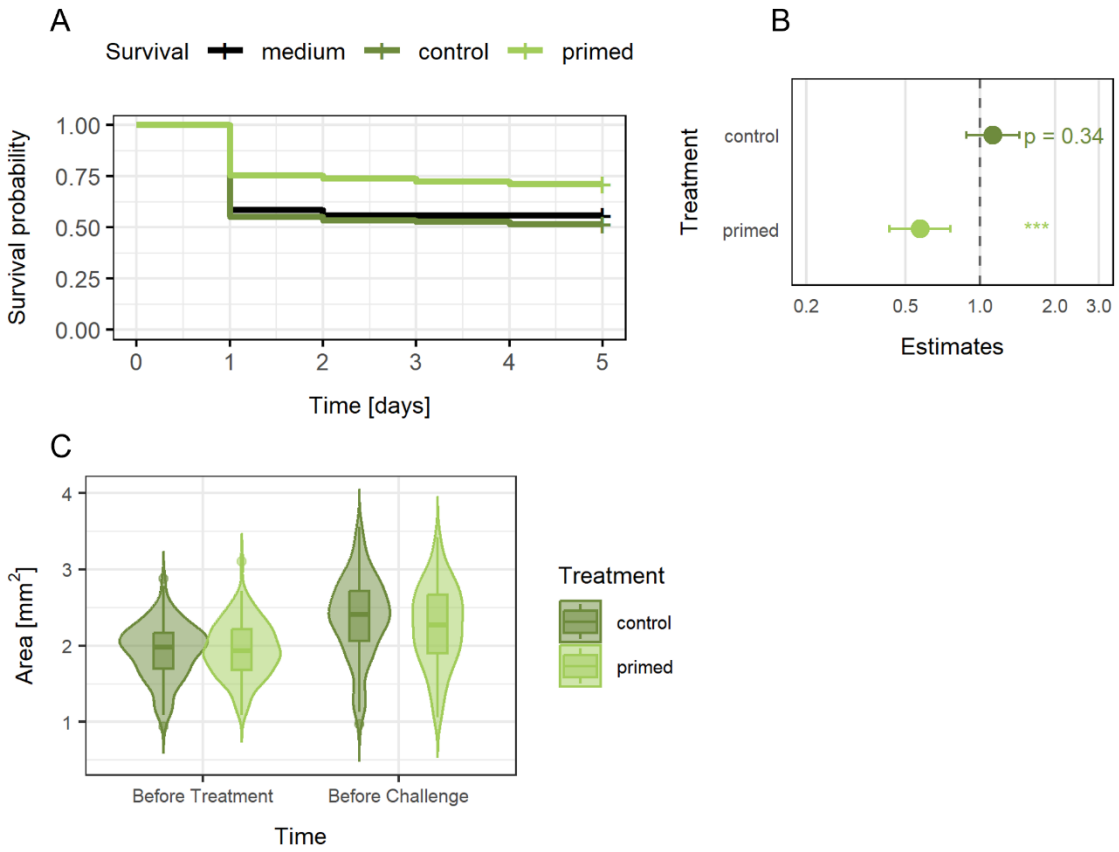

Fig 2: Infection survival and growth of *T. castaneum* larvae after priming. A Kaplan Meier curves displaying the survival of *T. castaneum* larvae exposed to either *Bt* medium diets (n =495), control diets (n =500), or priming diets (n =501) upon exposure to infectious *Btt* spores. **B** Forest plot representing the estimated fixed-effects coefficients of primed and control compared to medium (black, dashed line a 1.0). **C** Growth of *T. castaneum* larvae exposed to either priming (n = 132 larvae) or control (n = 135 larvae) diets. Larval size is given as their body area. The raw data for survival and growth can be found in S1 Table.

315 To analyze gene expression patterns in gut tissues from larvae that were either exposed to priming or
316 control diets we combined two approaches: DESeq2 was used to compare each gene's expression
317 between priming and control at each time point [45], and WGCNA was used to construct gene co-
318 expression networks [47]. The number of differentially expressed genes (DEGs) between primed and
319 control larval gut tissues varied over time (Fig 3A), peaking at 24 h post-exposure with approximately 5
320 – 10 times as many DEGs compared to the other time points. In unchallenged larvae, more genes were
321 down-regulated in primed larval gut tissues after five days, whereas upon challenge with life *Btt* most
322 DEGs were up-regulated in primed larval gut tissues (Fig 3A). We also used the normalized gene
323 expression of all DEGs identified between treatments across time points and performed hierarchical
324 clustering, as well as principal component analysis (Fig 3B, S2 Fig). The samples clustered well by their
325 group (time and treatment, Fig 3B). Moreover, samples that were exposed to *Btt* spores (both primed
326 and control) clustered together. However, the primed samples after three and 24 hours clustered
327 closest with one another and the *Btt* exposed samples, whereas the primed samples after 5 days
328 clustered closest with the control samples. This shows, that early after priming and exposure to *Btt*
329 spores many genes are similarly strongly expressed. When comparing the identity of DEGs between
330 priming and control across the different time points, there was little overlap indicating that the priming
331 response generally is dynamic (Fig 3C, D).

332

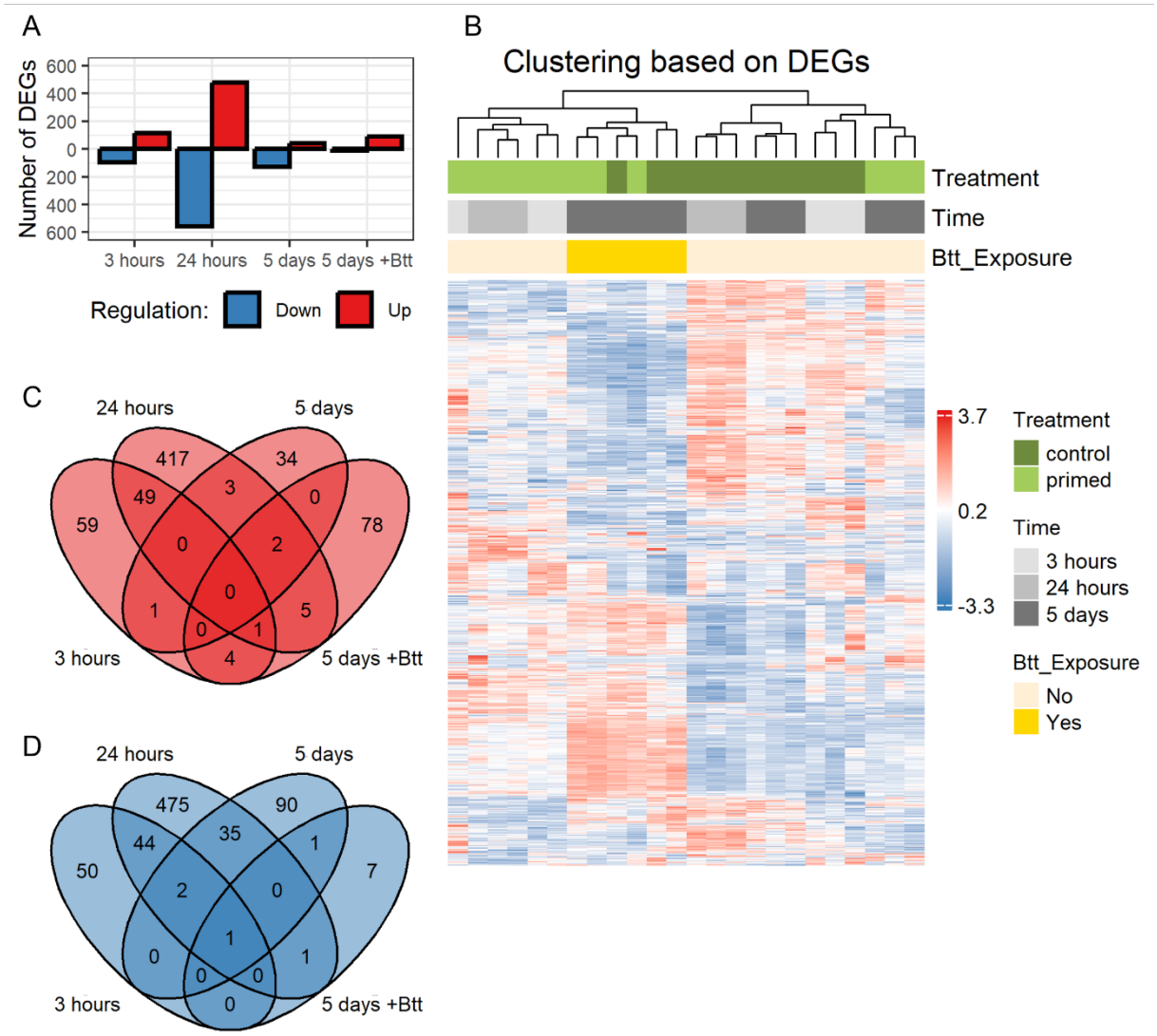

Fig 3: Overview of the results from the DESeq2 analysis. A Number of differentially expressed genes in guts from *T. castaneum* larvae exposed to priming *vs.* control diets (Down = lower expressed in primed guts, Up = higher expressed in primed guts), three hours, 24 hours and 5 days after priming without and with challenge (+Btt), analyzed with DESeq2 (Differentially expressed: Down in primed guts = Log2FC < -0.5, FDR adjusted p < 0.05, Up in primed guts = Log2FC > 0.5, FDR adjusted p < 0.05). **B** Heatmap representing the hierarchical clustering of the normalized gene expression for DEGs across all samples. Rows represent all DEGs identified in this study at all timepoints between primed and control larvae. Columns represent individual triplicate samples grouped by treatment, Time and exposure to infectious *Btt* spores (No = not exposed, Yes = exposed). Colors of the cells indicate the correlation of gene expression for a gene (row), in a sample (column). **C and D** Venn diagram for significantly up- (**C**) and down-regulated (**D**) genes between primed and control larval gut tissues at the different timepoints (three hours, 24 hours, 5 days, 5 days exposed to *Btt* spores). Overlapping areas represent shared DEGs between timepoints. The raw count data from the RNA-sequencing run can be found in S2 table.

After filtering out genes with low expression levels across samples, 10,814 genes of the total 17,052 genes remained for WGCNA. The WGCNA analysis identified 25 modules, with module 1 containing 2,262 genes and module 25 containing 36 genes (S3 Fig). Similarly, to the differential gene expression analysis, *Btt* exposed samples from control and priming treatment clustered well together upon

351 Pearson correlation of the module eigengene values with the samples grouped by treatment and time
352 (S4 Fig). We then went on and statistically compared the module eigengene (ME) values at each
353 timepoint between primed and control samples. Only the 24-hour and 5-day time points displayed
354 statistically different ME values. After 24 hours, 7 modules displayed statistically different ME values
355 (FDR adjusted $p < 0.05$) between primed and control samples (Modules 1, 2, 8, 11, 13, 14, 17, Fig 4).
356 Module 8 was excluded as no GO terms could be identified in this module. The gene ontology (GO)
357 analysis of key modules revealed that biological processes associated with protein synthesis and folding
358 are upregulated in primed larval guts after 24 hours compared to controls, suggesting an increased
359 cellular stress response (Fig 4A, Module 1). Additionally, priming was associated with elevated
360 expression of genes involved in cell cycle regulation and nuclear DNA-related processes, further
361 indicating an increased stress state (Fig 4A, Module 13). Conversely, Modules 2, 11, 14, and 17
362 comprised genes downregulated in primed larvae relative to controls (Fig 4B). Processes such as lipid
363 catabolism and gene expression were reduced, which, in conjunction with the upregulation of protein
364 folding genes, may indicate endoplasmic reticulum (ER) stress. Downregulation of genes involved in
365 cellular signaling, including the BMP signaling pathway, paired with upregulation of cell cycle genes,
366 which might suggest shifts in cell differentiation. Notably, at the 5-day mark, Modules 14 and 17 also
367 exhibited significant differences in module eigengene (ME) values between primed and control guts
368 (Fig 4B). These WGCNA findings underscore the potential for priming-induced stress, prompting us to
369 combine transcriptomic insights with transmission electron microscopy (TEM) to investigate
370 ultrastructural changes associated with gene expression dynamics in response to priming.

371

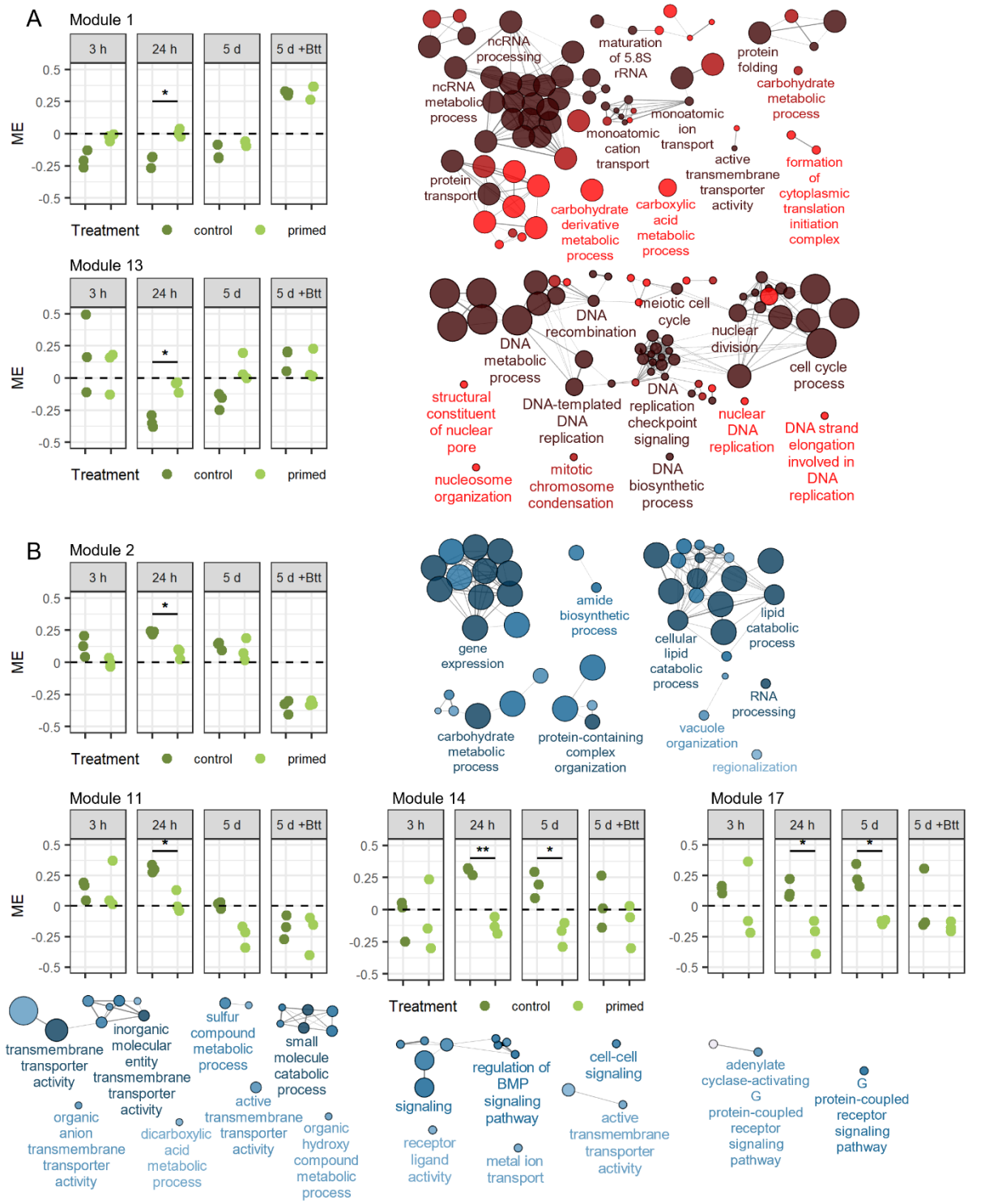

Fig 4 WGCNA modules with a significantly different module eigengene value (FDR adjusted p < 0.05) between larvae exposed to priming or control diets. The dot plots display module eigengene values (y-axis) vs samples grouped by timepoint (h = hours, d = days) and priming treatment (x-axis). Asterisks display significance levels (* = p <=0.05, ** = p <= 0.01). The networks represent Biological Processes contained in the modules identified with ClueGO. Only significantly enriched terms are included (Holm-Bonferroni adjusted p < 0.05). Each node represents a GO term. Node labels are based on the most significant GO term of a group of interconnected GO terms. Node size represents the number of genes mapped to the node. Node color reflects significance level (Dark = highly significant, bright = less significant). Edges connect nodes and define groups based on shared genes (Kappa >= 0.4). **A** Modules 1 and 13 show higher module eigengene values for primed compared to control. **B** Modules 2,

11, 14, and 17, show lower module eigengene values for primed compared to control. WGCNA analysis is based on the data found in S2 and S3 Table.

The early priming response is characterized by damage-associated stress responses and an up-regulation of immune genes

As early as three hours after the exposure to the priming diets, the electron micrographs revealed a tattered peritrophic matrix (compare Fig 5A and 5D, arrowheads) and a higher abundance of apoptotic cells in the gut of primed larvae (compare Fig 5C and Fig 5F). We also observed an increase of membrane vesicles in the gut lumen after priming (compare Fig 5B and 5E). Fitting these pathology observations in the gut of primed larvae, many DEGs at this time point are related to metabolic processes (Fig 5G). Up-regulated genes in primed larvae fell into the category of serine-type endopeptidases (S4 Table: 3 h: Category = “Proteases”), but also a ceramide synthase and genes encoding for proteins involved in intracellular protein degradation were significantly higher expressed (S4 Table: 3 h: Category = “Lipid metabolism” and “Proteases”). Most down-regulated genes fell into categories of lipid and carbohydrate catabolic processes (Fig 5G, S4 Table: 3 h: Category = “Lipid metabolism” and “Glycosidases”). None of the modules derived from the WGCNA analysis displayed significantly different ME values three hours after priming, but most up-regulated genes identified by DESeq2 clustered into module 1, and most down-regulated genes clustered into module 2.

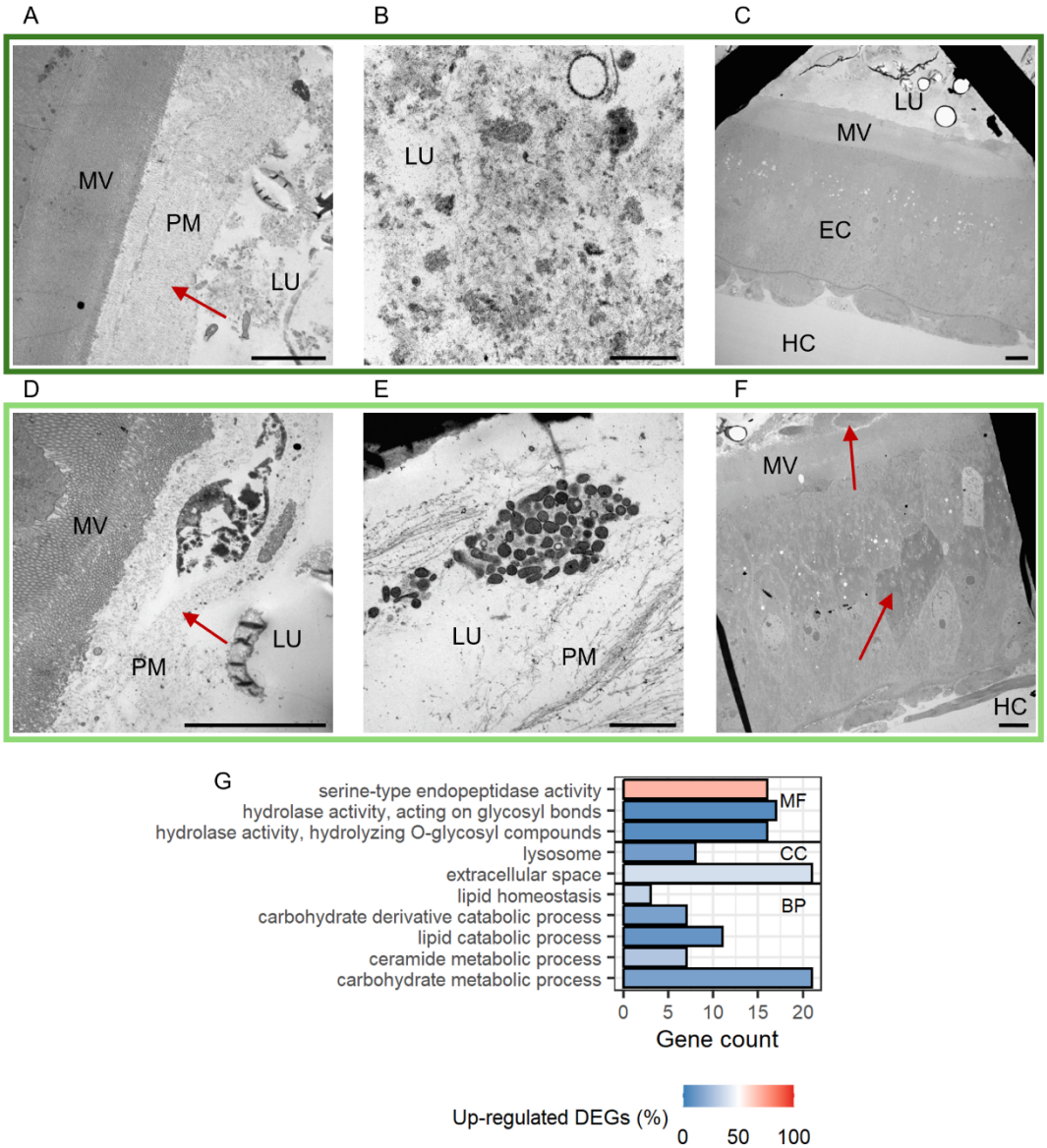

Fig 5: Differences between larvae exposed to control (*Btt Δ p188*) and priming (*Btt*) diets 3 hours after exposure. **A – F** Electron micrographs of control larvae (A-C) and primed larvae guts (D-F). Micrographs were chosen based on similar position and depth of sections between treatments. LU = gut lumen, MV = microvilli, PM = peritrophic matrix, EC = epithelial cell, HC = hemocoel. Red arrows: A, D = highlighting differences in peritrophic matrix, F = apoptotic cells. Scale bars: A = 5 µm, B = 1 µm, C = 5 µm, D = 5 µm, E = 1 µm, F = 5 µm. **G** GO term enrichment analysis for differentially expressed genes (DESeq2) between primed and control larval guts. Only GO terms with a significant enrichment are displayed (FDR adjusted $p < 0.05$). MF = Molecular Function, CC = Cellular Compartment, BP = Biological Process. The x-axis shows the number of genes that belong to a GO term, the color gradient indicates the ratio of down- (blue) and up-regulated (red) genes identified with DESeq2.

In line with the peak in the number of DEGs after 24 hours, we detected stronger differences in the gut ultrastructure between primed and control larvae at this time point. In primed larvae, the tattered

414 peritrophic matrix and increased apoptosis detected after three hours persisted. Still, additional
415 structures in the gut lumen and in between microvilli appeared, which seem to be membrane residues
416 originating from gut epithelial cells (compare Fig 6A and 6D, arrowheads). Both WGCNA and DESeq2
417 revealed down-regulated genes in primed larval gut tissue that clustered into GO categories of lipid
418 and carbohydrate catabolic processes (Fig 4B: Module 2, Fig 6G, S4 Table: 24 h: Category = "Lipid
419 metabolism" and "Glycosidases"), which coincides with the disturbance of cellular membranes and the
420 PM on the ultrastructure level. At the same time, genes encoding for chitin synthase and ceramide
421 synthase were up-regulated, possibly counteracting the degradation of cellular membranes and the
422 PM. Also, mitochondria in the epithelial cells of primed larval guts showed signs of stress, such as
423 elongated shapes and shrinkage (compare Fig 6B and E, arrowheads). Additionally, we observed an
424 increased number of autolysosomes, presumably due to the increased degeneration of mitochondria
425 (compare Fig 6C and 6F). This stress on the ultrastructure level within the epithelial cells was also
426 reflected by a high number of genes that clustered into GO terms that involve the synthesis,
427 modification, transport, and degradation of proteins, especially in the endoplasmic reticulum, which
428 was again indicated by both DESeq2 and WGCNA (Fig 4A: Module 1, Fig 5G, S4 Table: 24 h: Category =
429 "ER stress"). We also found the GO term "defense response to bacterium" to be significantly enriched
430 in primed larval guts at this time point (Fig 6G). Within this category are two gene copies of *Attacin*,
431 *Coleoptericin,* and *Defensin*, respectively, as well as a gene encoding for an inducible metalloprotease
432 inhibitor (S4 Table: 24 h: Category = "Immune"). Also, two genes encoding for peptidoglycan
433 recognition receptors were differentially regulated. Further significant modules identified by WGCNA
434 with higher gene expression profiles in primed larval gut tissues contained genes that participate in the
435 recombination, replication, and repair of DNA and genes associated with cell cycle processes in the
436 nucleus (Fig 4A: Module 13). Modules that were associated with a lower gene expression profile
437 contained genes involved in transmembrane transporter activities and cell-to-cell signaling (Fig 4B:
438 Modules 11, 14, and 17).

439

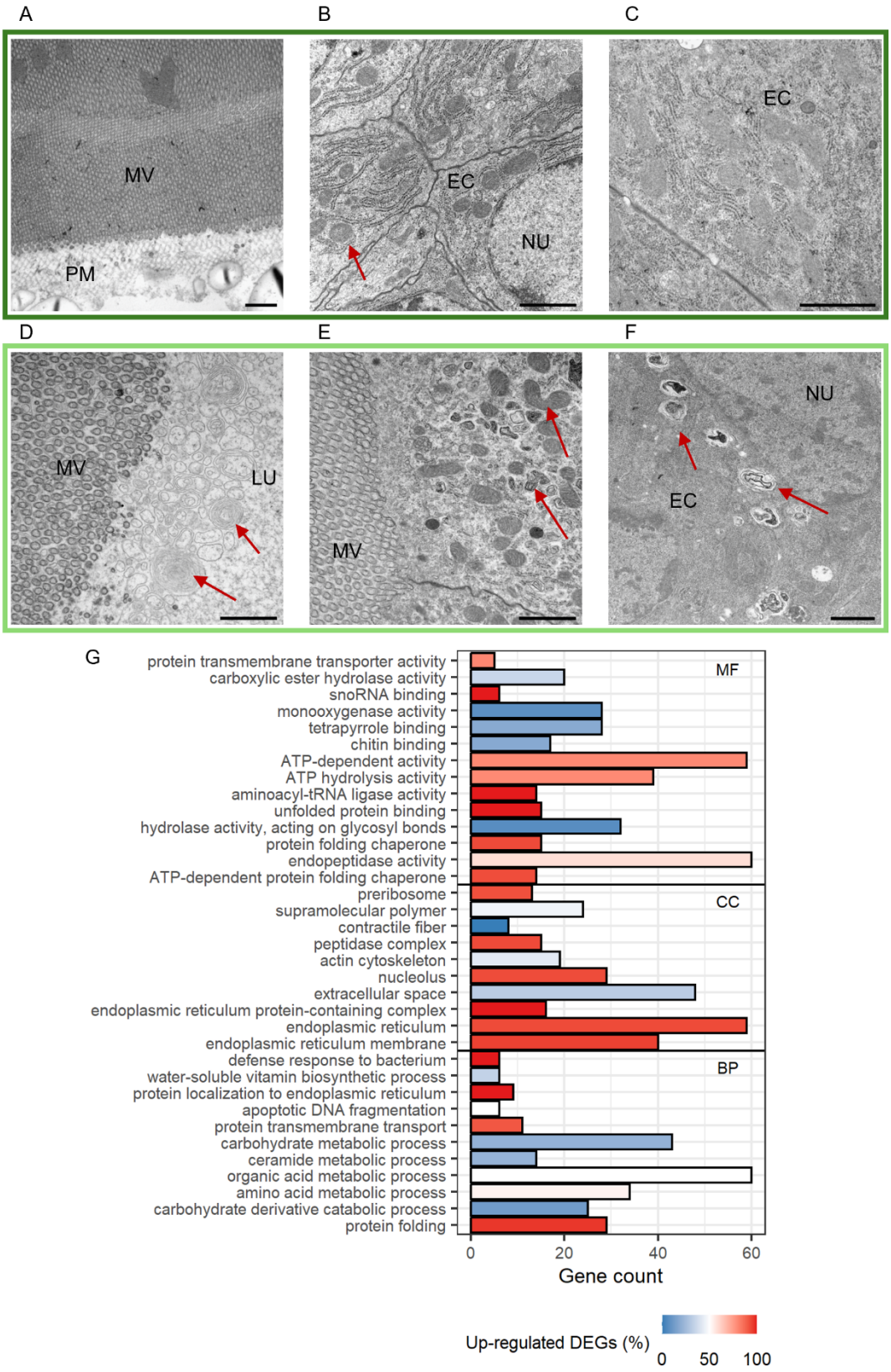

Fig 6: Differences between larvae exposed to control (*Btt* Δ*p188*) and priming (*Btt*) diets 24 hours after exposure. A – F Electron micrographs of control larvae (A-C) and primed larvae guts (D-F). Micrographs were chosen based on similar position and depth of sections between treatments. LU = gut lumen, MV = microvilli, PM = peritrophic matrix, EC = epithelial cell, NU = nucleus. Red arrows: A, D = "normal" (A) and "stressed" (D) mitochondria, E = autolysosomes, F = putative membrane residues originating from epithelial cells. Scale bars: A

- F = 5 µm. **G** GO term enrichment analysis for differentially expressed genes (DESeq2) between primed and control larval gut tissues. For details, see Fig 5.

Reduced gene expression differences after 5 days, while stress signs at the ultrastructural level persist

After 5 days, we still observed structural differences in the gut of primed larvae, such as the above-mentioned unusual shapes of mitochondria or the increased abundance of autolysosomes (compare Fig 7A and 7D). Additionally, we detected the occurrence of signs of stress in the ER of epithelial cells, namely the degeneration of ribosomes and even the degradation of the ER in primed larvae (Fig 7D). The most prominent change, however, was the microvilli (MV) swelling in primed larval guts (compare Fig 7B, E, C, F). These swellings occurred towards the tip of the MV and finally led to the extrusion of MV debris. Genes that were down-regulated in primed larvae at this time point encoded, among others, for proteins that are part of the cytoskeletal architecture or are involved in detoxification processes (Fig 7G, S4 Table: 5d: Category = “Cytoskeletal”, “Monooxygenases”). After 24 hours, genes encoding for transmembrane transporter activity were down-regulated as well as revealed by WGCNA and DESeq2 (Fig 4B: Modules 14 and 17, Fig 7G, S4 Table: 5d: Category = “Transporters”).

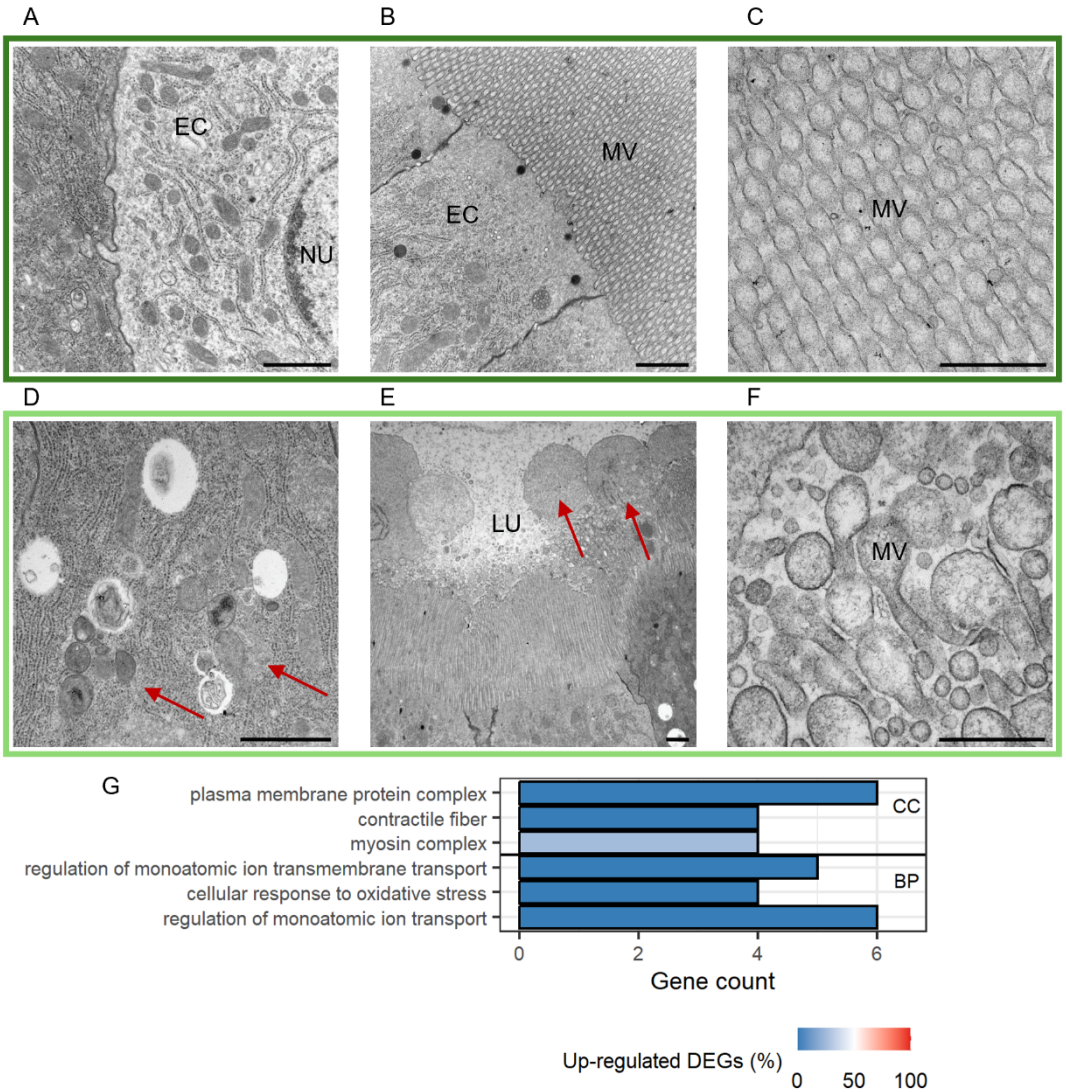

Fig 7: Differences between larvae that had been exposed to control (*Btt Δ p188*) and priming (*Btt*) diets 5 days after exposure. A – F Electron micrographs of control larvae (A-C) and primed larvae guts (D-F). Micrographs were chosen based on similar position and depth of sections between treatments. LU = gut lumen, MV = microvilli, EC = epithelial cell, NU = nucleus. Red arrows: D = stressed endoplasmic reticulum, E = swollen microvilli. Scale bars: A = 1 µm, B = 1 µm, C = 500 nm, D = 1 µm, E = 1 µm, F = 500 nm. **G** GO term enrichment analysis for differentially expressed genes (DESeq2) between primed and control larval gut tissues. For details, see Fig 5.

Upon exposure to life *Btt*, primed guts show higher expression of genes involved in detoxification processes

Five days after exposure to the priming or control diets, the guts of larvae that were exposed to *Btt* spores showed signs of infection in all samples. Vegetative *Btt* cells (Fig 8A and D), lysosomal structures (Fig 8B), and intracellular vesicles (Fig 8E) were present in both control and primed larvae. In some gut sections, we detected an increased number of apoptotic cells (Fig 8C), whereas other sections displayed a stressed MV rim (Fig 8F). Primed and control larval guts hardly differed, as the biggest influence on gut integrity seemed to be the number of germinated *Btt* cells, which varied largely even within the treatment. In line with this, the number of DEGs between primed and control larvae was the lowest among the investigated time points (Fig 3A). The only significant GO term containing down-regulated genes was “beta-glucosidase activity”, including an acidic chitinase (Fig 8G). Genes that were up-regulated in primed larvae upon *Btt* exposure encoded for detoxification enzymes, which were down-regulated in non-exposed larvae at this timepoint, lipid binding proteins and proteins containing leucine-rich repeats (Fig 8G, S4 Table: 5d_E: Category = “Detoxification”, ”Lipid binding”, “LRR”). Similar to three hours after priming, none of the modules derived from the WGCNA analysis displayed significantly different module eigengene values after the spore exposure treatment.

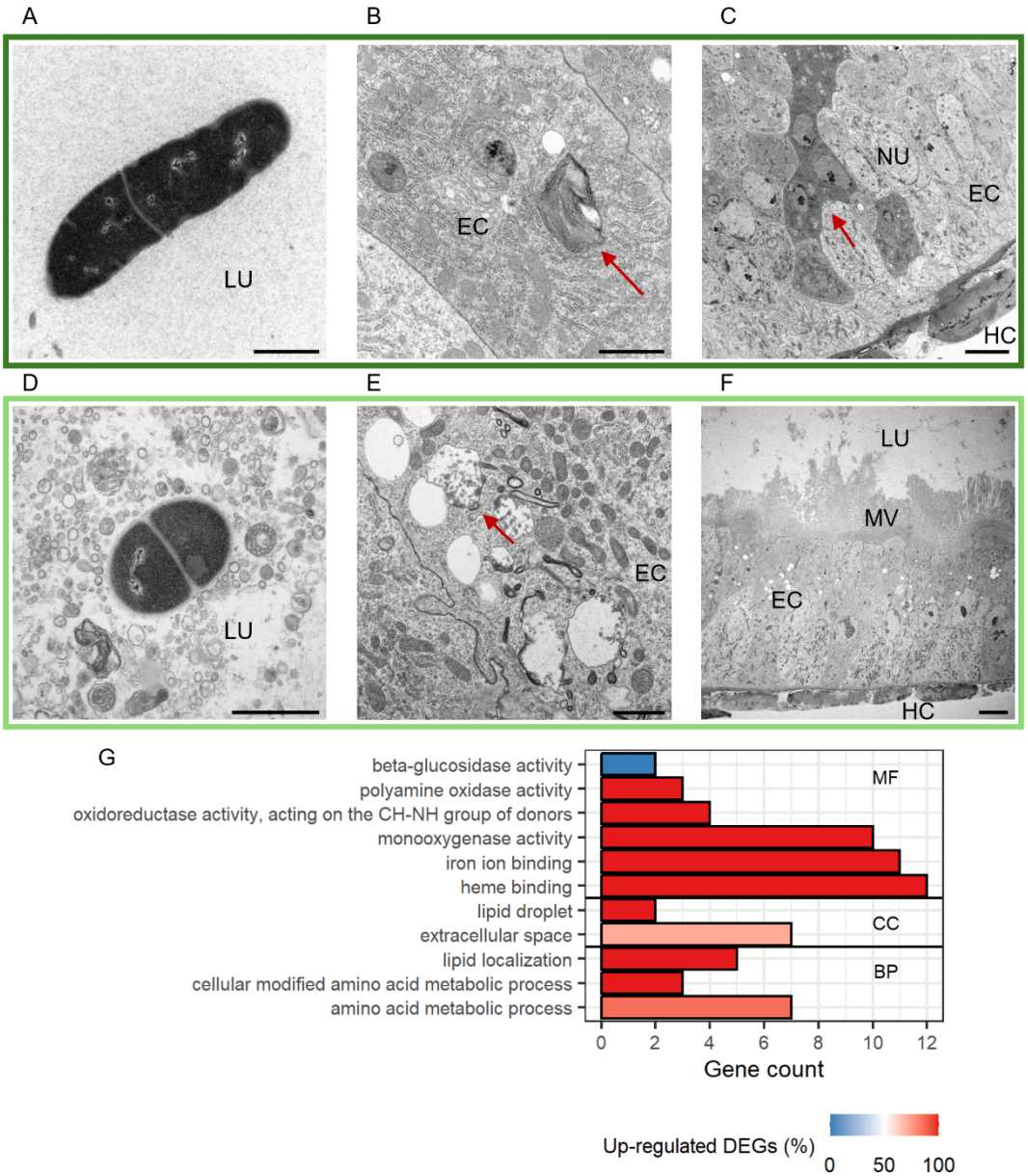

Fig 8: Differences between larvae that had been exposed to control (*Btt Δ p188*) and priming (*Btt*) diets 5 days after exposure and 4 hours after exposure to infectious *Btt* spores. A – F Electron micrographs of control larvae (A-C) and primed larvae guts (D-F). Micrographs were chosen based on similar position and depth of sections between treatments. LU = gut lumen, MV = microvilli, EC = epithelial cell, NU = nucleus, HC = hemocoel. Red arrows: B = lysosomal structure, C = apoptotic cells, E = intracellular vesicles. Scale bars: A = 1 µm, B = 1 µm, C = 5 µm, D = 1 µm, E = 1 µm, F = 5 µm. **G** GO term enrichment analysis for differentially expressed genes (DESeq2) between primed and control larval gut tissues. For details, see Fig 5.

497 **Priming-associated damage in the gut is likely caused by virulence**

498 **factors present in the priming diet**

499 When we compared the proteomes of priming (*Btt*) and control (*Btt Δ p188*) centrifuged, sterile filtered
500 media supernatants, the only significantly differentially enriched protein group was a
501 Sphingomyelinase C, which showed increased expression in the priming inducing *Btt* supernatant (S5A
502 Fig). As expected, proteins that are encoded on the Cry-toxin carrying 188 kb plasmid were below
503 detection limit in the *Btt Δ p188* control supernatants, where this plasmid was removed. Among those
504 proteins were the crystal toxins Cry3Aa and Cry15Aa (S5A Table). Sphingomyelinase C is encoded on
505 the same plasmid. The low expression level detected in 3 of 4 control media might be explained by
506 another homologous Sphingomyelinase encoded on the chromosome and containing identical peptide
507 fragments. Upon imputation of missing values, Cry15A, Cry3Aa and Sphingomyelinase C were among
508 the few protein groups that were significantly higher expressed in priming spent culture media
509 supernatants (Fig 9, S5B Fig, S5B and S5C Tables). Another virulence factor, Chitinase D, that was
510 previously found to be differentially expressed in *Btt* compared to another *Bt* strain, was highly
511 expressed in both, control and priming supernatants [32].

512

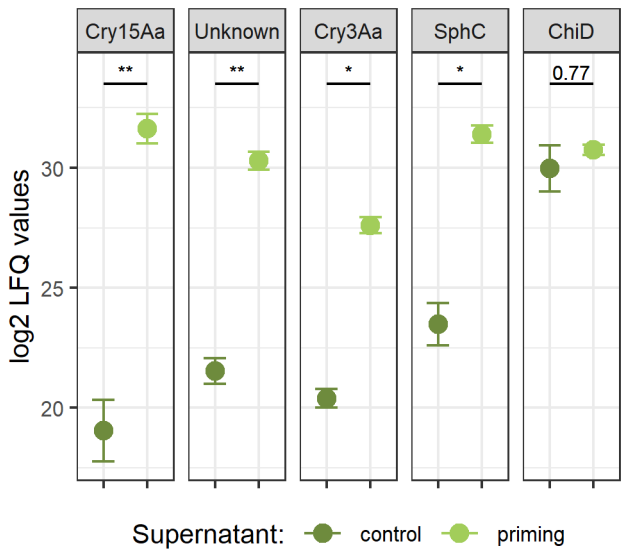

Fig 9: Exemplary proteome expression differences between priming (*Btt*) and control (*Btt Δ p188*) spent culture media supernatants. Depicted are the mean values of the normalized and log2-transformed label-free quantification values after imputation for missing values (n = 4). Error bars represent the standard error. ** = p value < 0.01, * = p value < 0.05. SphC = Sphingomyelinase C, ChiD = chitinase D.

520 # Discussion

521 To gain insights into the dynamic responses following oral immune priming in the insect gut, we
522 combined electron microscopy and RNA-sequencing of guts of primed and control *T. castaneum* larvae
523 at different timepoints and upon exposure to life *Btt* spores. Additionally, we used mass spectrometry
524 to characterize the cues present in the priming inducing spent media supernatants of *Btt* cultures. Our
525 results show a strong reaction in the primed gut associated with *Btt*-triggered tissue damage early after
526 priming, including the up-regulation of immune genes, that diminishes over time but enables a
527 targeted response upon re-encountering infective *Btt* spores.

528 The gut epithelium was strongly affected early after the exposure to the priming diet, as indicated by
529 damage in the peritrophic matrix and an increase in apoptotic cells and autolysosomes after three
530 hours (Fig 5D and 5F). After 24 hours, such damage was more pronounced; additionally, mitochondria
531 showed signs of stress or degraded. Membrane residues were shed into the gut lumen (Fig 6A-F).
532 Similar membrane and micro-vesicle shedding upon exposure to pore-forming toxins has been
533 reported in HeLa cells and mice and seems to aid in the repair of damaged cellular membranes [51,
534 52]. Overall, the observed changes in gut ultrastructure in primed larvae at these early time points
535 reflect the presence of virulence factors (e.g. Cry toxins, Chitinases, Sphingomyelinase C) in priming-
536 inducing *Btt* culture supernatants and resemble natural *Bt* infections [29, 30]. Chitinases break down
537 the chitinaceous peritrophic matrix, and Cry toxins, once dissolved and activated by midgut proteases,
538 bind to receptors on midgut epithelial cells, ultimately leading to cell death [29, 53, 54].
539 Sphingomyelinases further damage cellular membranes by hydrolyzing sphingomyelin to ceramide and
540 phosphorylcholine [55, 56]. In accordance with the increase of signs of damage after 24 hours, the
541 number of differentially expressed genes (DEGs) between primed and control larval gut tissues also
542 peaked at this time point. Among the DEGs were cysteine- and serine proteases, the main digestive
543 enzymes in *T. castaneum* [57]. In a study in *Tenebrio molitor*, oral exposure to Cry3Aa led to a similar
544 shift in the expression profiles of cysteine- and serine proteases [58]. Also, early work on the proteolytic

545 processing of Cry3Aa by insect gut enzymes indicated an influence of the gut enzyme composition on
546 Cry3Aa activity [59, 60]. After 24 hours, two serine protease inhibitors (serpins) were additionally
547 upregulated in primed larval guts, suggesting active regulation, especially for these proteases. Serpins'
548 tight regulation of these proteases might also be associated with their roles in insect immunity [61].
549 Genes encoding for glycosyl hydrolases family proteins were downregulated at the early time points
550 after priming. More than a third of the glycosyl hydrolases, which were downregulated after 24 hours,
551 are involved in chitin degradation. This, together with the upregulation of chitin synthase, could
552 indicate a strategy to suppress chitin catabolism in the presence of externally induced peritrophic
553 matrix damage. Genes involved in lipid metabolic processes were differentially regulated after priming
554 at the early timepoints as well. Ceramidases, sphingomyelinases, and lipases were mostly
555 downregulated. Downregulation of acid- and neutral sphingomyelinases in mammalian cell lines aids
556 regeneration upon exposure to pore-forming toxins [62]. The ceramide synthase *CerS6* gene and a gene
557 encoding for a serine palmitoyltransferase, important in sphingomyelin synthesis, were upregulated in
558 primed larvae at these early time points. Sphingomyelins are major constituents of cellular membranes
559 but also play roles in endoplasmic reticulum (ER) homeostasis and immune signaling [63-66]. The
560 presence of sphingomyelinase C in priming-inducing supernatant, together with the differential
561 expression of sphingomyelin-associated genes and the occurrence of membrane residues in the gut
562 lumen of primed larvae after 24 hours, suggests a disturbance of lipid homeostasis in these guts. In the
563 intestines of cockroaches, it has been shown that ER stress and lipid homeostasis are connected, and
564 that disturbance increases the expression of pro-inflammatory genes [67]. At 24 hours post priming,
565 genes were up-regulated that are linked to such ER-associated stress. These included genes that encode
566 for membrane-spanning proteins in the ER [68-71] and genes encoding for components of the cytosolic
567 proteasome complex, necessary for the correct degradation of proteins [72]. Also, genes that are
568 known to play important roles in the unfolded protein response (UPR), a cellular stress response related
569 to ER stress, were up-regulated [73-77]. In *Aedes aegypti,* knockdown of UPR genes reduced the
570 survival upon treatment with Cry11Aa toxin [78]. Most of these genes clustered into module 1 in our

571 WGCNA analysis whose eigengene value was significantly higher in primed larvae than control larvae
572 after 24 hours (Fig 4A).

573 Cell cycle and checkpoint signaling genes were also higher expressed in the primed gut after 24 hours
574 compared to control guts (Fig 4A). Many genes involved in these processes have been reported to
575 correlate with ER stress, and the influence of ER stress on DNA integrity, repair and epigenetic changes,
576 is a topic of active research [79-81]. Further, differences in gene expression in the cell cycle could hint
577 at divergent stem cell decisions upon priming, as observed upon pathogen exposure in Drosophila [82].
578 Unresolved ER stress leads to increased autophagy and cell death, signs we detected in the
579 ultrastructure of primed larvae at these early time points. Generally, genes involved in gene expression
580 were expressed lower in primed larvae (Fig 4B). In contrast, tRNA synthetase- and ribosome genes were
581 up-regulated (Fig 6G), potentially reflecting an increased demand in protein synthesis while controlling
582 for unbalanced gene expression [83]. Two genes encoding peptidoglycan recognition proteins (PGRP)
583 were differentially regulated after 24 hours. PGRP-SA was up- and PGRP-LB down-regulated. The same
584 direction of expression for these two PGRPs has previously been observed following septic infections
585 in *T. castaneum* using the Gram-positive bacterium *Micrococcus luteus* [84]. Additionally, Gram-positive
586 bacteria targeting antimicrobial peptides (AMPs) were up-regulated after 24 hours [85-87], indicating
587 a strong immune reaction 24 hours after exposure to the priming diet. Interestingly, genes encoding
588 for monooxygenases, a group of enzymes that are known to be involved in detoxification processes and
589 are overexpressed in some *Bt*-resistant insects [88, 89], were mostly down-regulated after 24 hours.
590 Overall, the differential regulation of genes in the gut involved in immunity, peptidase activity, and
591 monooxygenase activity 24 hours after priming resembles the gene expression patterns found in whole
592 larvae shortly after *Btt* exposure in other work [19, 31].

593 Five days after priming, guts showed additional stress in the ER and the degradation of ribosomes (Fig
594 7D). An even more notable phenomenon was the formation of enlarged microvilli (MV) heads (compare
595 Fig 7B, E vs. 7C, F). Such MV “blebs” have been described in rats and can contain catalytically active
596 enzymes with regulatory properties against microbes [90-92]. If and how MV “blebs” could affect *Btt*

597 proliferation upon exposure to the spore diets is still unclear and an interesting question to follow up.
598 Despite the obvious ultrastructural differences between the guts of primed and control larvae, the gene
599 expression profiles were more similar compared to the early time points. Most DEGS were
600 downregulated in primed guts (Fig 3A), including several genes encoding for proteins involved in the
601 cytoskeletal structure of cells, which correlates with the aberrant appearance of the MV (Fig 7G). Also,
602 several transmembrane transporter genes were down-regulated (Figs 7H and 4B). Similar transporters
603 are reported to function as receptors for Cry toxins. However, the reported putative functional
604 receptors for *T. castaneum* were unaffected [93-95]. Genes encoding for monooxygenases were mostly
605 downregulated after 24 hours. As detoxifying enzymes are costly to maintain and, therefore, under
606 strict regulation [96], the lower expression level in primed larval guts after 24 hours might have
607 persisted to 5 days after.

608 The guts of primed and control larvae hardly differed on the ultrastructural level after exposure to
609 infectious *Btt* spores (Fig 8A-F). In both cases, the gut epithelium was damaged, and vegetative cells of
610 *Btt* were visible. The microvilli rim was degraded, and we found many apoptotic cells within the
611 epithelia of primed and control guts. Overall, the effects of the infection seem so strong that they
612 override smaller, priming-associated differences. Also, the number of DEGs was the lowest upon
613 exposure to life *Btt* (Fig 3A). However, most of these DEGs were upregulated in primed guts (Fig 3A).
614 Interestingly, many of their gene products have been described to bind to pathogen-derived molecules
615 and invoke immune signaling. Examples are genes encoding for apolipophorinI/II, proteins containing
616 leucine-rich repeats, odorant binding receptors, and a scavenger receptor [97-102]. Some of these
617 genes have also been reported to be upregulated in *T. castaneum* upon *Btt* exposure in other studies
618 [31, 103]. A gene encoding for Arylphorin, which has been correlated with *Bt* resistance in a
619 Lepidopteran host by acting as a mitogen, was the second highest upregulated gene after *Btt* exposure
620 in primed larvae compared to control larvae [104, 105]. In contrast to 24 hours after priming and 5 days
621 after priming without exposure to *Btt* spores, monooxygenases, a Glutathion-S-transferase, and a
622 Peroxiredoxin were upregulated in primed larvae after exposure to *Btt* spores. Overall, four hours after

623 *Btt* spore exposure, primed larvae possessed an increased abundance of transcripts for genes involved
624 in the binding and detoxification of foreign/pathogen compounds and cellular regeneration, which
625 could imply a strategy to prevent damage done by the virulence factors of *Btt*.

626 For the first time, we described in detail the changes in the gut of *T. castaneum* larvae upon oral
627 immune priming. In mosquitos and bean bugs, the microbiome breaches the epithelial cell lining,
628 thereby influencing immune cell differentiation [15, 27]. Indeed, the microbiome in our system is
629 needed for successful oral immune priming as well [26], and a change in its composition is described
630 upon priming [28]. However, we here could not detect any signs of bacterial breaching in the gut
631 epithelia on the ultrastructural level upon priming, and it is debated whether *Btt* breaches the gut
632 before host death [106]. Pinaud *et al.* [17] showed that in snails, oral immune priming leads to a shift
633 from a cellular immune response upon the first encounter with the parasite to a humoral response
634 after the second encounter. In their system, however, the *Schistosoma* parasite forms sporocysts that
635 develop within the host tissue, representing a different pathogenesis than that of *Btt*. These works
636 highlight the differences in the investigated host–parasite models and reflect the diversity of immune
637 priming phenomena in invertebrates [107]. In our case, virulence factors in the sterile filtered spent
638 culture media supernatant of *Btt* induce a stress state in the gut of *T. castaneum* that resembles an
639 actual infection at the ultrastructural (compare Figs 5A-F + 6A-F + 8A-F) and gene expression level. This
640 stress state initially induces an immune response that diminishes over time, but upon re-infection with
641 live *Btt* spores results in up-regulation of protective genes against *Btt*. Greenwood *et al.* [31] found an
642 increased immune response in primed *T. castaneum* larvae 6 hours after exposure to life *Btt* using
643 whole larvae. It is known that *T. castaneum* is able to build immune memory upon septic infection [14,
644 16]. Thus, investigating the potential crosstalk between the gut epithelium and the hemocoelic side
645 would be interesting. The identified changes in the gut might induce hemocyte migration or
646 differentiation or influence the gene expression profile of fat body tissue. This could lead to systemic
647 immune responses and memory, which might aid protection against oral *Btt* infection and potentially
648 also septic infection.

649 With respect to the five immune memory criteria as worked out by Pradeu and Du Pasquier [108],
650 immune priming in *T. castaneum* meets the following: it is specific to a certain degree both via the
651 septic and oral route [14, 18], it might enable a faster response as indicated by the early up-regulation
652 of protective genes in the gut found in this study as well as the up-regulation of immune genes at whole
653 larval level found by Greenwood et al. [31]. Protection in orally primed larvae lasts for at least 5 days,
654 as shown in this study, and up to 8 days, as in some septic studies, and can be transmitted to subsequent
655 generations [14, 23]. The initial priming response in the gut diminishes the gene expression level over
656 five days, indicating extinction (Fig 3A + B).

657 But how could memory be formed in the insect gut epithelium? Work by Liu X et al. [81] in *Drosophila*
658 showed that pathogenic microbes, in contrast to the normal microbiota, activate additional molecular
659 pathways. This causes stem cells to differentiate into enteroendocrine cell types, changing the
660 epithelial cell composition in the gut epithelium. Such changes might provide a type of memory that is
661 based on epithelial cell structure. Accordingly, our WGCNA analysis identified differences in gene
662 expression in the cell cycle and related processes 24 hours after priming (Fig 4A). Also, it is known from
663 other systems that inflammatory memory exists in epithelial tissue in the form of chromatin
664 rearrangements [5, 6]. Interesting candidates for the induction of memory and specificity of oral
665 immune priming in our system are toxins such as Cry3Aa that are unique to certain strains of *Bt*. The
666 damage done by these toxins, combined with the shifts in microbiome composition, could provide the
667 stimuli needed to invoke epigenetic or architectural changes in the gut epithelium that lead to memory
668 in non-immune tissue.

669 On this basis, the insect model might be important for future work on immune memory, which is not
670 simply understood as a property of innate or adaptive immune cells in isolation. It seems rather a
671 property of interacting cells and tissues that, on their own or in combination, might be able to form
672 memory.

Acknowledgements

We thank Kathrin Brüggemann, Ilka Rauch and Anke Große Brinkhaus for their technical assistance.

Funding

We acknowledge funding by the Deutsche Forschungsgemeinschaft (DFG, German Research Foundation) within the Research Training Group GRK 2220 "Evolutionary Processes in Adaptation and Disease," project number 281125614 to JK and partial funding within CRC TRR 212 (NC^3) – project number 316099922 to JK.

References

[1] Kurtz J. Specific memory within innate immune systems. *Trends in Immunology.* 2005; 26(4): 186-192.

[2] Murphy K and Weaver C. Janeway's Immunobiology. New York: Garland Science. 2017.

[3] Ferreira AV, Domiguéz-Andrés J, Netea MG. The Role of Cell Metabolism in Innate Immune Memory. *J Innate Immun.* 2022; 14: 42-50.

[4] Saeed S, Quintin J, Kerstens HHD, Rao NA, Aghajanirefah A, Matarese F, et al. Epigenetic programming of monocyte-to-macrophage differentiation and trained innate immunity. *Science.* 2014; 345(6204).

[5] Naik S, Larsen SB, Gomez NC, Alaverdyan K, Sendoel A, Yuan S, et al. Inflammatory memory sensitizes skin epithelial stem cells to tissue damage. *Nature*. 2017; 550: 475-480.

[6] Hamada A, Torre C, Drancourt M, Ghigo E. Trained Immunity Carried by Non-immune Cells*. Front. Microbiol*. 2019; 9: 3225.

[7] Kurtz J, Franz K. Evidence for memory in invertebrate immunity. *Nature*. 2003; 425: 37-38.

[8] Sadd BM, Schmid-Hempel P. Insect Immunity Shows Specificity in Protection upon Secondary Pathogen Exposure. *Current Biology*. 2006; 16: 1206-1210.

[9] Milutinovic B, Fritzlar S, Kurtz J. Increased Survival in the Red Flour Beetle after Oral Priming with Bacteria-Conditioned Media. *J Innate Immun*. 2014; 6: 306-314.

[10] Eleftherianos I, Marokhazi J, Millichap PJ, Hodgkinson AJ, Sriboonlert A, Constant RH, Reynolds SE. Prior infection of *Manduca sexta* with non-pathogenic *Escherichia coli* elicits immunity to pathogenic *Photorhabdus luminescens*: Roles of immune-related proteins shown by RNA interference. *Insect Biochem Mol Biol*. 2006; 36: 517-525.

[11] Wu G, Zhao Z, Liu C, Qiu L. Priming *Galleria mellonella* (Lepidoptera: Pyralidae) Larvae With Heat-Killed Bacterial Cells Induced an Enhanced Immune Protection Against *Photorhabdus luminescens* TT01 and the Role of Innate Immunity in the Process. *J Econ Entomol*. 2014; 107(2): 559-569.

[12] Pham LN, Dionne MS, Shirasu-Hiza M, Schneider DS. A Specific Primed Immune Response in Drosophila Is Dependent on Phagocytes. *PLoS Pathog*. 2007; 3(3): e26.

[13] Lanz-Mendoza H, Gálvez D, Contreras-Garduño. The plasticity of immune memory in invertebrates. *J Exp. Biol.* 2024; 227(Suppl_1):jeb246158.

[14] Roth O, Sadd BM, Schmid-Hempel P, Kurtz J. Strain-specific priming of resistance in the red flour beetle, *Tribolium castaneum*. *Proc Biol Sci*. 2009; 276(1654): 145-151.

[15] Rodrigues J, Brayner FA, Alves LC, Dixit R, Barillas-Mury C. Hemocyte Differentiation Mediates Innate Immune Memory in *Anopheles gambiae* Mosquitoes. *Science*. 2010; 329(5997): 1353-1355.

[16] Ferro K, Peuß R, Yang W, Rosenstiel P, Schulenburg H, Kurtz J. Experimental evolution of immunological specificity. *PNAS.* 2019; 116(41):20598-20604.

[17] Pinaud S, Portela J, Duval D, Nowacki FC, Olive M-A, Allienne J-F, et al. A Shift from Cellular to Humoral Responses Contributes to Innate Immune Memory in the Vector Snail *Biomphalaria glabrata*. *PLoS Pathog*. 2016; 12(1): e1005361.

[18] Futo M, Sell MP, Kutzer MAM, Kurtz J. Specificity of oral immune priming in the red flour beetle *Tribolium castaneum. Biol Lett*. 2017; 13(12): 20170632.

[19] Behrens S, Peuß R, Milutinovic B, Eggert H, Esser D, Rosenstiel P, et al. Infection routes matter in population-specific responses of the red flour beetle to the entomopathogen *Bacillus thuringiensis. BMC Genomics*. 2014; 15(1):445.

[20] Mikonranta L, Mappes J, Kaukoniitty M, Freitak D. Insect immunity: oral exposure to a bacterial pathogen elicits free radical response and protects from a recurring infection. *Front Zool*. 2014; 11:23.

[21] Moreno-García M, Vargas V, Ramírez-Bello I, Hernández-Martínez G, Lanz-Mendoza H. Bacterial Exposure at the Larval Stage Induced Sexual Immune Dimorphism and Priming in Adult *Aedes aegypti* Mosquitoes. *PLoS One*. 2015; 10(7): e0133240.

[22] Norouzitallab P, Biswas P, Baruah K, Bossier P. Multigenerational immune priming in an invertebrate parthenogenetic Artemia to a pathogenic *Vibrio campbellii. Fish Shellfish Immunol*. 2015; 42(2):426-9.

[23] Schulz NKE, Sell MP, Ferro K, Kleinhölting N, Kurtz J. Transgenerational Developmental Effects of Immune Priming in the Red Flour Beetle *Tribolium castaneum. Front Physiol*. 2019; 10: 98.

[24] Moret Y. "Trans-generational immune priming": specific enhancement of the antimicrobial immune response in the mealworm beetle, *Tenebrio molitor*. *Proc Biol Sci*. 2006; 273(1592):1399-405.

[25] Shi ZH, Lin YT, Hou YM. Mother-derived trans-generational immune priming in the red palm weevil, *Rhynchophorus ferrugineus* Olivier (Coleoptera, Dryophthoridae). *Bull Entomol Res*. 2014; 104(6):742-50.

[26] Futo M, Armitage SAO, Kurtz J. Microbiota Plays a Role in Oral Immune Priming in *Tribolium castaneum*. *Front Microbiol*. 2016; 6(6): 1383.

[27] Jang S, Ishigami K, Mergaert P, Kikuchi Y. Ingested soil bacteria breach gut epithelia and prime systemic immunity in an insect. *PNAS*. 2024; 121(11):e2315540121.

[28] Korša A, Lo LK, Gandhi S, Bang C, Kurtz J. Oral Immune Priming Treatment Alters Microbiome Composition in the Red Flour Beetle *Tribolium castaneum*. *Front Microbiol*. 2022; 13(13): 793143.

[29] Raymond B, Johnston PR, Nielsen-LeRoux C, Lereclus D, Crickmore N. *Bacillus thuringiensis*: an impotent pathogen? *Trends Microbiol*. 2010; 18(5): 189-194.

[30] de Maagd RA, Bravo A, Crickmore N. How *Bacillus thuringiensis* has evolved specific toxins to colonize the insect world. *Trends Genet*. 2001; 17(4):193-9.

751 [31] Greenwood JM, Milutinović B, Peuß R, Behrens S, Esser D, Rosenstiel P, et al. Oral immune priming
752 with *Bacillus thuringiensis* induces a shift in the gene expression of *Tribolium castaneum* larvae. *BMC*
753 *Genomics*. 2017; 18(1): 329.

754 [32] Länger ZM, Baur M, Korša A, Eirich J, Lindeza AS, Zanchi C, et al. Differential proteome profiling of
755 bacterial culture supernatants reveals candidates for the induction of oral immune priming in the red
756 flour beetle. *Biol Lett*. 2023; 19(11): 20230322.

757 [33] Hughes CS, Moggridge S, Müller T, Sorensen PH, Morin GB, Krijgsveld J. Single-pot, solid-phase-
758 enhanced sample preparation for proteomics experiments. *Nat Protoc*. 2019; 1:68-85.

759 [34] Sindlinger J, Schön S, Eirich J, Kirchgäßner S, Finkemeier I, Schwarzer D. Investigating Peptide-
760 Coenzyme A Conjugates as Chemical Probes for Proteomic Profiling of N-Terminal and Lysine
761 Acetyltransferases. *ChemBioChem*. 2022; e202200255.

762 [35] Tyanova S, Temu T, Cox J. The MaxQuant computational platform for mass spectrometry-based
763 shotgun proteomics. *Nat Protoc*. 2016; 11(12):2301–19.

764 [36] Andrews, S. FastQC: A Quality Control Tool for High Throughput Sequence Data. 2010;
765 http://www.bioinformatics.babraham.ac.uk/projects/fastqc/.

766 [37] Kim D, Paggi JM, Park C, Bennett C, Salzberg SL. Graph-based genome alignment and genotyping
767 with HISAT2 and HISAT-genotype. *Nat Biotechnol.* 2019; 37:907–915.

768 [38] Pertea M, Pertea GM, Antonescu CM, Chang T-C, Mendell JT, Salzberg SL. StringTie enables
769 improved reconstruction of a transcriptome from RNA-seq reads . *Nat Biotechnol*. 2015; 33(3):290-295.

770 [39] Liao Y, Smyth GK, Shi W. featureCounts: an efficient general purpose program for assigning
771 sequence reads to genomic features. *Bioinformatics*. 2014; 30(7):923-30.

772 [40] R Core Team. _R: A Language and Environment for Statistical Computing_. R Foundation for
773 Statistical Computing, Vienna, Austria. 2023; https://www.r-project.org/.

[41] Wickham H. *ggplot2: Elegant Graphics for Data Analysis*. *Springer-Verlag New York*. 2016; ISBN 978-3-319-24277-4, https://ggplot2.tidyverse.org.

[42] Ritchie ME, Phipson B, Wu D, Hu Y, Law CW, Shi W, et al. limma powers differential expression analyses for RNA-sequencing and microarray studies. *Nucleic Acids Res*. 2015; 43(7):e47.

[43] Bates D, Mächler M, Bolker B, Walker S. Fitting Linear Mixed-Effects Models Using lme4. *Journal of Statistical Software*. 2015; 67(1), 1–48.

[44] Therneau TM, Grambsch PM. Modeling survival data: extending the Cox model. *Springer Verlag*. 2000.

[45] Therneau TM. A Package for Survival Analysis in R. 2020; https://CRAN.R-project.org/package=survival.

[46] Love M I, Huber W, Anders S. Moderated estimation of fold change and dispersion for RNA-seq data with DESeq2. *Genome biology*. 2014; 15(12): 1-21.

[47] Wu T, Hu E, Xu S, Chen M, Guo P, Dai Z. clusterProfiler 4.0: A universal enrichment tool for interpreting omics data. *The Innovation*. 2021; 2(3), 100141.

[48] Langfelder P, Horvath S. WGCNA: an R package for weighted correlation network analysis. *BMC Bioinformatics*. 2008; 559.

[49] Shannon P, Markiel A, Ozier O, Baliga NS, Wang JT, Ramage D, et al. Cytoscape: a software environment for integrated models of biomolecular interaction networks. *Genome research*. 2003; 13(11):2498–504.

[50] Bindea G, Mlecnik B, Hackl H, Charoentong P, Tosolini M, Kirilovsky A, et al. ClueGO: a Cytoscape plug-in to decipher functionally grouped gene ontology and pathway annotation networks. *Bioinformatics*. 2009; 25(8):1091-1093.

796 [51] Keyel PA, Loultcheva L, Roth R, Salter RD, Watkins SC, Yokoyama WM, Heuser JE. Streptolysin O
797 clearance through sequestration into blebs that bud passively from the plasma membrane. *J Cell Sci*.
798 2011; 124(14): 2414-23.

799 [52] Romero M, Keyel M, Shi G, Bhattacharjee P, Roth R, Heuser JE, Keyel PA. Intrinsic repair protects
800 cells from pore-forming toxins by microvesicle shedding. *Cell Death Differ*. 2017; 24(5): 798-808.

801 [53] Malovichko YV, Nizhnikov AA, Antonets KS. Repertoire of the *Bacillus thuringiensis* Virulence
802 Factors Unrelated to Major Classes of Protein Toxins and Its Role in Specificity of Host-Pathogen
803 Interactions. *Toxins*. 2019; 11(6) 347.

804 [54] Palma L, Muñoz D, Berry C, Murillo J, Caballero P. *Bacillus thuringiensis* Toxins: An Overview of
805 Their Biocidal Activity. *Toxins*. 2014; 6(12): 3296-325.

806 [55] Openshaw AEA, Race PR, Monzó HJ, Vázquez-Boland J-A, Banfield MJ. Crystal Structure of SmcL, a
807 Bacterial Neutral Sphingomyelinase C from Listeria. *J Biol Chem*. 2005; 280(4): 35011-7.

808 [56] Celandroni F, Salvetti S, Senesi S, Ghelardi E. *Bacillus thuringiensis* membrane-damaging toxins
809 acting on mammalian cells. FEMS *Microbiol Lett*. 2014; 361(2): 95-103.

810 [57] Morris K, Lorenzen MD, Hiromasa Y, Tomich JM, Oppert C, Elpidina EN, et al. *Tribolium castaneum*
811 larval gut transcriptome and proteome: A resource for the study of the coleopteran gut. *J Proteome*
812 *Res*. 2009; 8(8): 3889-98.

813 [58] Oppert B, Dowd SE, Bouffard P, Li L, Conesa A, Lorenzen MD, et al. Transcriptome profiling of the
814 intoxication response of *Tenebrio molitor* larvae to *Bacillus thuringiensis* Cry3Aa protoxin. *PLoS One*.
815 2012; 7(4): e34624.

816 [59] Carroll J, Li J, Ellar DJ. Proteolytic processing of a coleopteran-specific delta-endotoxin produced
817 by *Bacillus thuringiensis var. tenebrionis. Biochem J*. 1989; 261(1): 99-105.

818 [60] Herrnstadt C, Soares GG, Wilcox ER, Edwards DL. A new strain of *Bacillus thuringiensis* with activity
819 against coleopteran insects. *Nature Biotech*. 1986; 4: 305-308.

820 [61] Shakeel M, Xu X, De Mandal S, Jin F. Role of serine protease inhibitors in insect-host-pathogen
821 interactions. *Arch Insect Biochem Physiol*. 2019, 102(3):e21556

822 [62] Schoenauer R, Larpin Y, Babiychuk EB, Drücker P, Babiychuk VS, Avota E, et al. Down-regulation of
823 acid sphingomyelinase and neutral sphingomyelinase-2 inversely determines the cellular resistance to
824 plasmalemmal injury by pore-forming toxins. *FASEB J*. 2019; 33(1): 275-285.

825 [63] Han J, Kaufman RJ. The role of ER stress in lipid metabolism and lipotoxicity. *J Lipid Res*. 2016;
826 57(8): 1329 -1338.

827 [64] Lee M, Lee SY, Bae Y-S. Functional roles of sphingolipids in immunity and their implication in
828 disease. *Exp Mol Med*. 2023; 55(6): 1110-1130.

829 [65] Piña F, Yagisawa F, Obara K, Gregerson JD, Kihara A, Niwa M. Sphingolipids activate the endoplasmic
830 reticulum stress surveillance pathway. *J Cell Biol*. 2018; 217(2): 495-505.

831 [66] Sidak-Loftis LC, Rosche KL, Pence N, Ujczo JK, Hurtado J, Fisk EA, et al. The Unfolded-Protein
832 Response Triggers the Arthropod Immune Deficiency Pathway. *mBio*. 2022; 13(4): e0070322.

833 [67] Fang W, Chen Q, Li J, Liu Y, Zhao Z, Shen Y, et al. Endoplasmic Reticulum Stress Disturbs Lipid
834 Homeostasis and Augments Inflammation in the Intestine and Isolated Intestinal Cells of Large Yellow
835 Croaker (*Larimichthys crocea*). *Front Immunol.* 2021; 19(12): 738143.

836 [68] Moretti F, Bergman P, Dodgson S, Marcellin D, Claerr I, Goodwin JM, et al. TMEM41B is a novel
837 regulator of autophagy and lipid mobilization. *EMBO Rep*. 2018; 19(9): e45889.

838 [69] Christodoulou A, Maimaris G, Makrigiorgi A, Charidemou E, Lüchtenborg C, Ververis A, et al.
839 TMEM147 interacts with lamin B receptor, regulates its localization and levels, and affects cholesterol
840 homeostasis. *J Cell Sci*. 2020; 133(16): jcs245357.

841 [70] Zhao Y, Hu J, Miao G, Qu L, Wang Z, Li G, et al. Transmembrane Protein 208: A Novel ER-Localized
842 Protein That Regulates Autophagy and ER Stress. *PLoS One*. 2013; 8(5): e64228.

843 [71] Li C, Wei J, Li Y, He X, Zhou Q, Yan J, et al. Transmembrane Protein 214 (TMEM214) Mediates
844 Endoplasmic Reticulum Stress-induced Caspase 4 Enzyme Activation and Apoptosis. *J Biol Chem*. 2013;
845 288(24): 17908-17.

846 [72] Qu J, Zou T, Lin Z. The Roles of the Ubiquitin–Proteasome System in the Endoplasmic Reticulum
847 Stress Pathway. *Int J Mol Sci*. 2021; 22(4): 1526.

848 [73] Ibrahim IM, Abdelmalek DH, Elfiky AA. GRP78: A cell's response to stress. *Life Sci*. 2019; 226: 156-
849 163.

850 [74] Marzec M, Eletto D, Argon Y. GRP94: an HSP90-like protein specialized for protein folding and
851 quality control in the Endoplasmic Reticulum. *Biochim Biophys Acta*. 2012; 1823(3): 774-787.

852 [75] Ni M, Lee AS. ER chaperones in mammalian development and human diseases. *FEBS Lett*. 2007;
853 581(19): 3641-51.

854 [76] Dejgaard S, Nicolay J, Taheri M, Thomas DY, Bergeron JJM. The ER Glycoprotein Quality Control
855 System. *Curr Issues Mol Biol*. 2004; 6(1): 29-42.

856 [77] Sevier CS, Kaiser CA. Ero1 and redox homeostasis in the endoplasmic reticulum. *Biochim Biophys*
857 *Acta*. 2008; 1783(4): 549-56.

858 [78] Bedoya-Pérez LP, Cancino-Rodezno A, Flores-Escobar B, Soberón M, Bravo A. Role of UPR Pathway
859 in Defense Response of *Aedes aegypti* against Cry11Aa Toxin from *Bacillus thuringiensis. Int J Mol Sci*.
860 2013; 14(4): 8467-8478.

861 [79] Chow CY, Wolfner MF, Clark AG. Using natural variation in Drosophila to discover previously
862 unknown endoplasmic reticulum. *PNAS*. 2013; 110(22): 9013-8.

863 [80] Rendleman J, Cheng Z, Maity S, Kastelic N, Munschauer M, Allgoewer K, et al. New insights into
864 the cellular temporal response to proteostatic stress. *eLife*. 2018; 7: e39054.

865 [81] Dicks N, Gutierrez K, Michalak M, Bordignon V, Agellon LB. Endoplasmic reticulum stress, genome
866 damage, and cancer. *Front Oncol*. 2015; 5: 11.

867 [82] Liu X, Nagy P, Bonfini A, Houtz P, Bing XL, Yang X, Buchon N. Microbes affect gut epithelial cell
868 composition through immune-dependent regulation of intestinal stem cell differentiation. *Cell Rep*.
869 2022, 38(13):110572.

870 [83] Gonen N, Meller A, Sabath N, Shalgi R. Amino Acid Biosynthesis Regulation during Endoplasmic
871 Reticulum Stress Is Coupled to Protein Expression Demands. *iScience*. 2019; 19: 204-213.

872 [84] Koyama H, Kato D, Minakuchi C, Tanaka T, Yokoi K, Miura K. Peptidoglycan recognition protein
873 genes and their roles in the innate immune pathways of the red flour beetle, *Tribolium castaneum. J*
874 *Invertebr Pathol*. 2015; 132: 86-100.

875 [85] Tonk M, Knorr E, Cabezas-Cruz A, Valdés JJ, Kollewe C, Vilcinskas A. *Tribolium castaneum* defensins
876 are primarily active against Gram-positive bacteria. *J Invertbr Pathol*. 2015; 132: 208-215.

877 [86] Ntwasa M, Goto A, Kurata S. Coleopteran Antimicrobial Peptides: Prospects for Clinical
878 Applications. *Int J Microbiol*. 2012; 2012: 101989.

879 [87] Vertyporokh L, Wojda I. Expression of the insect metalloproteinase inhibitor IMPI in the fat body
880 of *Galleria mellonella* exposed to infection with *Beauveria bassiana. Acta Biochim Pol*. 2017; 64(2): 273-
881 278.

882 [88] Shabbir MZ, Yang X, Batool R, Yin F, Kendra PE, Li Z-Y. *Bacillus thuringiensis* and Chlorantraniliprole
883 Trigger the Expression of Detoxification Related Genes in the Larval Midgut of *Plutella xylostella. Front*
884 *Physiol*. 2021; 12: 780255.

885 [89] Vellichirammal NN, Wang H, Eyun S-I, Moriyama EN, Coates BS, Miller NJ, Siegfried BD.
886 Transcriptional analysis of susceptible and resistant European corn borer strains and their response to
887 Cry1F protoxin. *BMC Genomics*. 2015; 16(1):558.

888 [90] McConnell RE, Higginbotham JN, Shifrin Jr DA, Tabb DL, Coffey RJ, Tyska MJ. The enterocyte
889 microvillus is a vesicle-generating organelle. *J Cell Biol*. 2009; 185(7): 1285-98.

890 [91] Sauvanet C, Wayt J, Pelaseyed T, Bretscher A. Structure, Regulation, and Functional Diversity of
891 Microvilli on the Apical Domain of Epithelial Cells. *Annu Rev Cell Dev Biol*. 2015; 31: 593-621.

892 [92] Shifrin Jr DA, McConnell RE, Nambiar R, Higginbotham JN, Coffey RJ, Tyska MJ. Enterocyte
893 microvillus-derived vesicles detoxify bacterial products and regulate epithelial-microbial interactions.
894 *Curr Biol*. 2012; 22(7): 627-31.

895 [93] Güney G, Cedden D, Hänniger S, Heckel DG, Coutu C, Hegedus DD, et al. Silencing of an ABC
896 transporter, but not a cadherin, decreases the susceptibility of Colorado potato beetle larvae to *Bacillus*
897 *thuringiensis ssp. tenebrionis* Cry3Aa toxin. *Arch Insect Biochem Physiol*. 2021; 108(2): e21834.

898 [94] Contreras E, Benito-Jardón M, López-Galiano MJ, Real MD, Rausell C. *Tribolium castaneum* immune
899 defense genes are differentially expressed in response to *Bacillus thuringiensis* toxins sharing common
900 receptor molecules and exhibiting disparate toxicity. *Dev Comp Immunol*. 2015; 50(2): 139-45.

901 [95] Pauchet Y, Bretschneider A, Augustin S, Heckel DG. A P-Glycoprotein Is Linked to Resistance to the
902 *Bacillus thuringiensis* Cry3Aa Toxin in a Leaf Beetle. *Toxins*. 2016; 8(12): 362.

903 [96] Misra JR, Horner MA, Lam G, Thummel CS. Transcriptional regulation of xenobiotic detoxification
904 in Drosophila. *Genes Dev*. 2011; 25(17):1796-806.

905 [97] Omae Y, Hanada Y, Sekimizu K, Kaito C. Silkworm Apolipophorin Protein Inhibits Hemolysin Gene
906 Expression of *Staphylococcus aureus* via Binding to Cell Surface Lipoteichoic Acids. *J Biol Chem*. 2013;
907 288(35): 25542-25550.

908 [98] Hanada Y, Sekimizu K, Kaito C. Silkworm Apolipophorin Protein Inhibits *Staphylococcus aureus*
909 Virulence. *J Biol Chem*. 2011; 286(45): 39360-39369.

910 [99] Ng A, Xavier RJ. Leucine-rich repeat (LRR) proteins: Integrators of pattern recognition and signaling
911 in immunity. *Autophagy*. 2011, 7(9):1082-4.

912 [100] Rong H, He X, Liu Y, Liu M, Liu X, Lu M. Odorant binding protein 18 increases the pathogen
913 resistance of the imported willow leaf beetle, *Plagiodera versicolora. Front Cell Infect Microbiol*. 2024;
914 14: 1360680.

915 [101] Benoit JB, Vigneron A, Broderick NA, Wu Y, Sun JS, Carlson JR, et al. Symbiont-induced odorant
916 binding proteins mediate insect host hematopoiesis. *eLife.* 2017; 6: e19535.

917 [102] Canton J, Neculai D, Grinstein S. Scavenger receptors in homeostasis and immunity. *Nat Rev*
918 *Immunol.* 2013; 13(9): 621-34.

919 [103] Contreras E, Rausell C, Real MD. Proteome Response of *Tribolium castaneum* Larvae to *Bacillus*
920 *thuringiensis* Toxin Producing Strains. *PLoS One*. 2013; 8(1): e55330.

921 [104] Hernández-Martínez P, Navarro-Cerrillo G, Caccia S, de Maagd RA, Moar WJ, Ferré J, et al.
922 Constitutive Activation of the Midgut Response to *Bacillus thuringiensis* in *Bt*-Resistant *Spodoptera*
923 *exigua. PLoS One*. 2010; 5(9): e12795.

924 [105] Castagnola A, Jackson J, Perera OP, Oppert C, Eda S, Jurat-Fuentes JL. Alpha-arylphorin is a
925 mitogen in the *Heliothis virescens* midgut cell secretome upon Cry1Ac intoxication. *PeerJ*. 2017; 5:
926 e3886.

927 [106] Zanchi C, Lindeza AS, Kurtz J. Comparative Mortality and Adaptation of a Smurf Assay in two
928 Species of Tenebrionid Beetles Exposed to *Bacillus thuringiensis*. *Insects*. 2020, 11(4):261.

929 [107] Milutinović B, Kurtz J. Immune memory in invertebrates. *Semin Immunol*. 2016, 28(4):328-42.

930 [108] Pradeu T, Du Pasquier L. Immunological memory: What's in a name? *Immunol Rev*. 2018,
931 283(1):7-20.

Supporting information captions

S1 Fig: Survival of *T. castaneum* larvae exposed to either control or priming diets from the EM and RNA-seq experiments. A Kaplan Meier curves displaying the survival of *T. castaneum* larvae exposed to either control diets (n =96 and 121), *Bt* medium diets (n =95 and 123) or priming diets (n =96 and 123) upon exposure to infectious *Btt* spores. **B** Forest plot representing the estimated fixed-effects coefficients of primed and control compared to medium (black, dashed line at 1.0).

S2 Fig: Principal component analysis. 3-dimensional PCA for differentially expressed genes identified with DESeq2. PC1 represents 40.34% variation, PC2 represents 15.25% variation and PC3 represents 9.66% variation.

S3 Fig: Hierarchical cluster tree of the weighted gene co-expression analysis. Each branch represents a single gene. Genes were clustered into modules based on their expression (unmerged), and closely related modules were merged based on their similarity in eigengene values (merged). The resulting modules are displayed in colors but were converted to numbers for later analysis.

S4 Fig: Pearson correlation of module eigengene values with control or priming treatments at the different timepoints. Cell color = pearson correlation coefficient. Asterisks = Significance of Student asymptotic p-value calculation (* if $p < 0.05$, ** if $p < 0.01$, *** if $p < 0.001$).

S5 Fig: Volcano plots for proteomic analysis. A Volcano plot for Btt vs Btt -cry supernatants without imputation for missing values. Plotted is the limma result for all protein groups that are at least in 3 of 4 samples of either Btt- or Btt -cry supernatants. X-axis represents the log2-fold-change (log2FC), the y-axis represents the negative log10-adjusted pvalue (-log10(adj.P.Val). The lines in the plot represent the chosen significance levels: The vertical lines are drawn at log2FC = -1/1, the horizontal line is drawn at -log10(0.05) = 1.301. Light green = significantly enriched protein groups. **. B** Volcano plot for Btt vs Btt -cry supernatants with imputation for missing values. Plotted is the limma result for th imputation of all protein groups that are at least in 3 of 4 samples of either Btt- or Btt -cry supernatants. X-axis represents the log2-fold-change (log2FC), the y-axis represents the negative log10-adjusted pvalue (-log10(adj.P.Val)). The lines in the plot represent the chosen significance levels: The vertical lines are drawn at log2FC = -1/1, the horizontal line is drawn at -log10(0.05) = 1.301. Light green = significantly enriched protein groups.

S1 Table: Survival and larval growth measurement data.

S2 Table: Raw count data from RNA sequencing.

S3 Table: Meta information about Samples from the RNA-Sequencing run.

S4 Table: Result for the differential gene expression analysis using DESeq2. Includes the results for the DESeq2 analyses at each timepoint between primed and control. Additionally contains categories used to group genes in biological context in the manuscript and the GO terms from the Clusterprofiler analyses.

S5 Table: Exemplary proteomics results for supernatants derived from *Btt ⊿ p188* (C) and Btt (P) cultures. A Log2 transformed label-free quantification (LFQ) values for candidate protein groups. **B** LFQ values upon imputation using the R package "imputeLCMD". **C** Limma statistics results for imputed values. (Full table in S6 Dataset).

S6 Table: Full proteomics table before and after imputation and Limma statistical analysis.

S1 Code: R Codes used for data analyses and figures.

985 # Data availability

986 Raw data for the RNA-sequencing experiment can be found at:
987 https://dataview.ncbi.nlm.nih.gov/object/PRJNA1174285?reviewer=1tvk9cnufn6k0qsbp3dqs2f56j.
988 This data will be made publicly available under the Bioproject: PRJNA1174285 upon publication of the
989 manuscript.

990

991 Raw data for the proteomics experiment can be found at
992 https://repository.jpostdb.org/preview/68712976967221def02b9b (with access key 4337 for
993 reviewers). This data will be made publicly available under the identifier JPST003396 upon publication
994 of the manuscript.

995